

Review

Photocatalysis and Li-Ion Battery Applications of {001} Faceted Anatase TiO₂-Based Composites

Anuja Bokare *  and Folarin Erogbogbo *

Department of Biomedical Engineering, San José State University, 1 Washington Square, San José, CA 95112, USA
* Correspondence: anujabokare@gmail.com (A.B.); folarin.erogbogbo@sjsu.edu (F.E.)

Abstract: Anatase TiO₂ are the most widely used photocatalysts because of their unique electronic, optical and catalytic properties. Surface chemistry plays a very important role in the various applications of anatase TiO₂ especially in the catalysis, photocatalysis, energy conversion and energy storage. Control of the surface structure by crystal facet engineering has become an important strategy for tuning and optimizing the physicochemical properties of TiO₂. For anatase TiO₂, the {001} crystal facets are the most reactive because they exhibit unique surface characteristics such as visible light responsiveness, dissociative adsorption, efficient charge separation capabilities and photocatalytic selectivity. In this review, a concise survey of the literature in the field of {001} dominated anatase TiO₂ crystals and their composites is presented. To begin, the existing strategies for the synthesis of {001} dominated anatase TiO₂ and their composites are discussed. These synthesis strategies include both fluorine-mediated and fluorine-free synthesis routes. Then, a detailed account of the effect of {001} facets on the physicochemical properties of TiO₂ and their composites are reviewed, with a particular focus on photocatalysis and Li-ion batteries applications. Finally, an outlook is given on future strategies discussing the remaining challenges for the development of {001} dominated TiO₂ nanomaterials and their potential applications.

Keywords: high energy TiO₂ facet; {001} TiO₂ facet; TiO₂-graphene composite; doping; photocatalysis; Li-ion battery anode



Citation: Bokare, A.; Erogbogbo, F. Photocatalysis and Li-Ion Battery Applications of {001} Faceted Anatase TiO₂-Based Composites. *J* **2021**, *4*, 500–530. <https://doi.org/10.3390/j4030038>

Academic Editor: Raed Abu-Reziq

Received: 31 July 2021

Accepted: 26 August 2021

Published: 6 September 2021

Publisher's Note: MDPI stays neutral with regard to jurisdictional claims in published maps and institutional affiliations.



Copyright: © 2021 by the authors. Licensee MDPI, Basel, Switzerland. This article is an open access article distributed under the terms and conditions of the Creative Commons Attribution (CC BY) license (<https://creativecommons.org/licenses/by/4.0/>).

1. Introduction

The rising demand for energy and the increase in environmental pollution have become extremely serious issues in recent years [1,2]. Harnessing the sun's energy to produce electricity and to remediate environmental pollution through the use of advanced nanomaterials has proven to be a promising solution to the world's energy crisis [3,4]. One of the first technologies that come to mind when discussing solar energy is photocatalysis. Photocatalysis relies on using the sunlight to promote the degradation of organic pollutants [5,6]. Among a wide spectrum of semiconductors, TiO₂ is the most efficient photocatalyst due to its chemical stability, non-toxicity, strong oxidizing power, biocompatibility, large surface area, corrosion resistivity and cost effectiveness [7–9].

The intense interest in titanium dioxide (TiO₂) as a photocatalyst has spurred the successful synthesis and extensive investigations of a variety of its crystal facets. Exploring the application of the high energetic {001} facets of titania is a recent venture in TiO₂ photocatalysis [10–13]. A natural anatase crystal typically can exhibit many crystal facets, as shown in Figure 1 [14,15]. Among them, {001} surfaces are highly desired because they are theoretically predicted to possess more active sites (five coordinated Ti⁺) and higher surface energy (0.90 J/m²) relative to other energetically more favorable facets such as {100} 0.53 J/m² or {101} 0.44 J/m² [16]. Both theoretical and experimental studies demonstrate that the photocatalytic activity of the anatase {001} facets is higher than that of the thermodynamically stable {101} facets [17–19]. Apart from photocatalytic studies, many other promising applications such as photo- or electrocatalysis, photoelectrochemical

or photovoltaic cells, lithium/sodium ion batteries, Li-S batteries and gas sensing can be significantly improved by morphological control and specifically exposed {001} facets on the surface [20–23]. Hence, more efforts are being made to synthesize TiO₂ nanomaterials with dominant high-energy {001} facets (TiO₂-001).

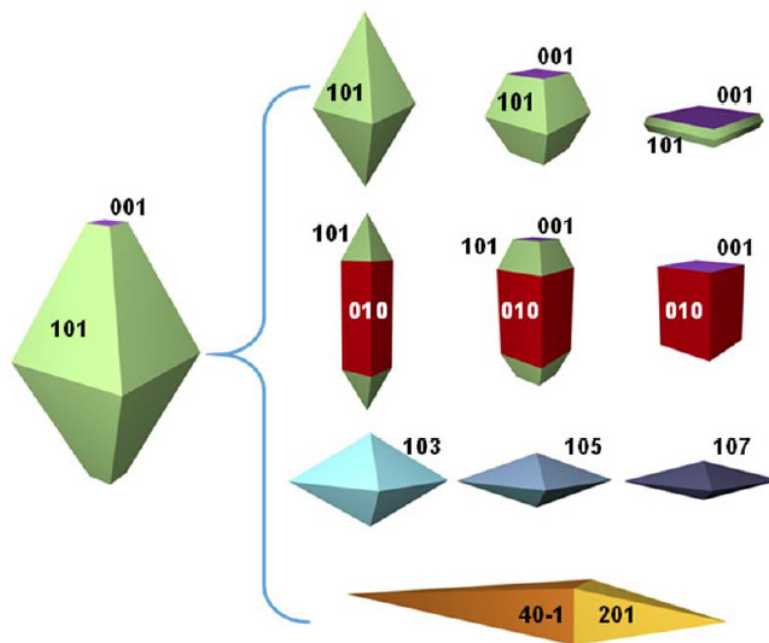


Figure 1. Equilibrium crystal shape of anatase TiO₂ through the Wulff construction and the evolved other shapes. (Reprinted with the permission of ref. [14], copyrights 2014 © American Chemical Society).

Even though the design and morphologically controlled synthesis of TiO₂-001 is considered to be a hot spot in scientific research, it still has some drawbacks like its wide band gap and high recombination rate [24]. These drawbacks can easily be overcome by coupling them with other materials to form TiO₂-001-based composites. For example, doping TiO₂-001 with metal (transition or rare-earth metal) or non-metal ions (C, F, S, N) can make them responsive to visible light [25]. Higher rates of recombination can be suppressed by noble metal deposition on the TiO₂-001 surface [26,27]. When coupled with carbon-based materials, TiO₂-001-based composites show excellent properties, such as high surface area, high absorptivity of dyes and high charge separation [28,29]. These properties make them applicable for many areas of science and technology ranging from adsorption, catalysis and photocatalysis to biomedicine, environmental monitoring and cleanup, energy conversion and storage, etc [30,31]. Hence, it is crucial to highlight the recent progress in the photocatalytic performance of TiO₂-based composites with {001} facets as a future energy material.

This review begins by explaining the role of {001} facets in improving the photocatalytic performance of TiO₂-001 photocatalysts. Then, a brief discussion is given on the modification of the catalysts by doping and coupling mechanisms. Further, we focus on the synthesis routes to obtain TiO₂-001 and modified TiO₂-001-based composites. This is then followed by the various applications of these composites which include environmental remediation by dye degradation, H₂ generation, CO₂ reduction and energy generation through Li-ion batteries. Finally, we present a conclusion and future scope of this emerging field which highlights the major challenges and some invigorating perspectives for future research.

2. Mechanism of Photoactivity Enhancement by {001} Facets in TiO₂

It has been widely recognized that the photocatalytic properties of TiO₂ nanomaterials can be altered by their crystal facets [32,33]. The opportunity to tune the surface properties

of anatase crystals by modifying the {001} exposed facets has been extensively reviewed in the last few years [34,35]. Anatase TiO₂ crystals with dominant {001} high energy facets possess characteristic surface configurations with plentiful dangling bonds and abundant surface defects [36]. Moreover, their surface chemistry can be easily modified, affecting adsorption, capacity, selectivity and surface reactivity [37]. In addition, the observed differences in the surface energy of crystallographic facets significantly affect the electronic and optical properties of the photocatalysts. Some of these properties are discussed below.

2.1. Properties of TiO₂-001 Surfaces for Photocatalysis

2.1.1. Dissociative Adsorption

In a recent study, it was found that the {010} facets could only absorb water molecules on its surface while the {001} facets could dissociate the water molecules, producing hydroxyl and other reactive radicals [38]. It is proposed that the {001} facets could also facilitate transfer of these charge carriers showing higher photocatalytic efficiency [39]. The dissociative adsorption of reactant molecules on {001} facets appears to reduce their activation energy and affect the reaction mechanism at the molecular level in the photocatalytic reaction. Similar chemical activity has also been observed in a wide range of organic species adsorption and other applications such as bacterial inactivation, verifying the unique surface chemistry of the {001} facet [40,41].

Many researchers have investigated the effect of dissociative adsorption on the photoactivity of TiO₂ crystals. They pointed out that the higher the percentage of {001} facets, the higher the photooxidation reactivity for similarly sized TiO₂ particles.

2.1.2. Charge Separation

Besides enhanced dissociative adsorption, charge separation of photogenerated charge carriers can also be mediated by {001} facets [42]. This can be mainly attributed to the unsaturated Ti atoms and defects (oxygen vacancy) present on the surface. The surface of TiO₂-001 nanomaterials exhibits high density of active, five-fold coordinated Ti atoms (Ti_{5c}) and wide Ti-O-Ti bond angles, as can be seen in Figure 2a [43]. This gives rise to the generation of a higher number of oxygen vacancies on the surface. Liu et al. proposed that oxygen deficiency within TiO₂-001 induces the specific surface reconstruction in combination with surface chemical species, which facilitates the interfacial electron transfer and e⁻/h⁺ charge separation [44].

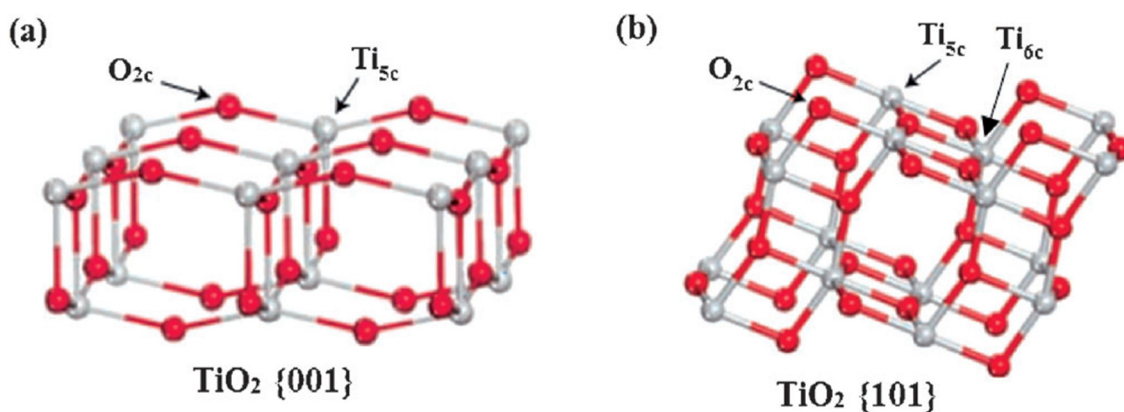


Figure 2. Schematic of surface atomic structure of anatase {001} and {101} crystal facets. (a) Large bond angles of Ti-O-Ti on the more reactive {001} surface. (b) Narrow bond angles of Ti-O-Ti on the less reactive {101} surface. (Reprinted with the permission of ref. [39], copyrights 2008 © Nature Publishing Group).

In addition, different atomic arrangements, surface energies and electronic structures associated with each family of TiO₂ facets drives selective migration of charge carriers towards different exposed facets. Generally, it is considered that the coordinately unsatu-

rated $O_{2c}-Ti_{5c}-O_{2c}$ bond on TiO_2 -001 surface is more selective for the oxidation of adsorbed species whereas {010} facets show selectivity for the reduction reactions (Figure 3a,b) [45,46]. Hence, ideal spatial separation on these 001 (oxidation) and {010} (reduction) sites on the TiO_2 nanoparticle reduces the recombination of photogenerated charge carriers, thus increasing the photocatalytic efficiency. Recently, Liberto et al. [36] evaluated the role of exposed {001} and {101} crystal facets in photocatalytic processes. They detected charge-trapping centers for Ti^{3+} and O^- ions by performing electron spin resonance spectroscopy and concluded that the concentration of trapped holes (O^- centers) increased with increasing amounts of {101} facets, whereas the amount of Ti^{3+} centers for trapped electrons increased with {001} facets (Figure 3e), thus confirming the efficient charge separation on TiO_2 -001 surfaces [47,48].

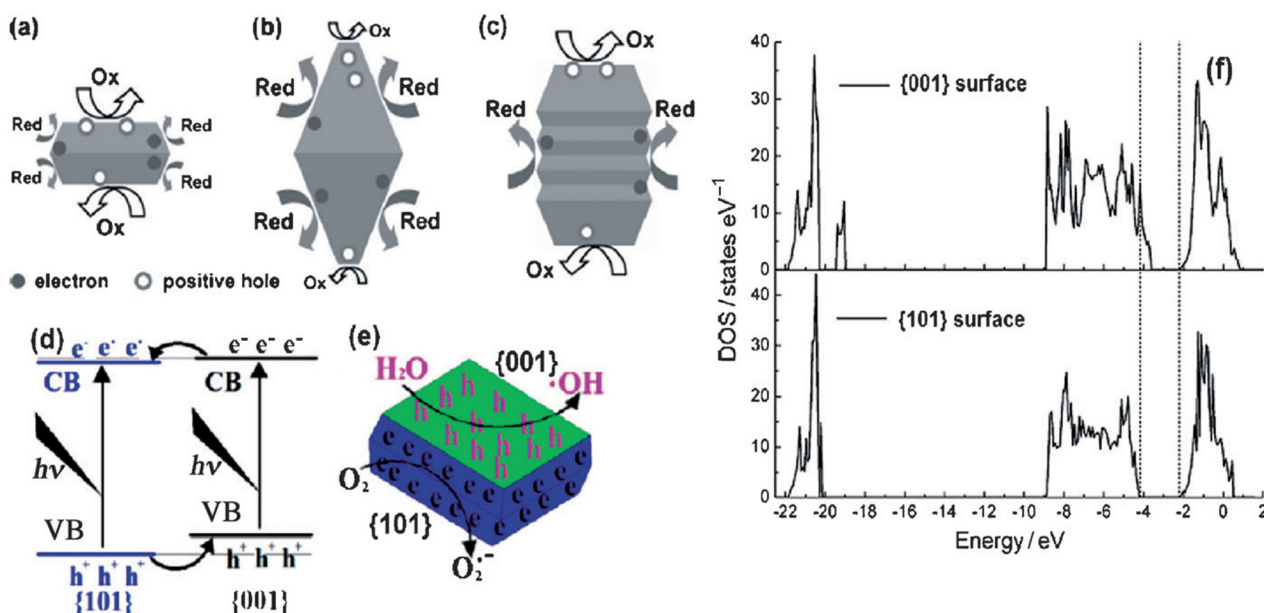


Figure 3. Schematic illustrations of spatial separation of redox sites on the anatase with exposed {001} and {101} crystal facets. (a–c) Different shapes of TiO_2 particle with a decahedral particle with {001} facets as oxidation sites and {101} facets as reducing sites. (Reprinted with the permission of ref. [49] copyrights 2009 © American Chemical Society). (d) Electronic band structures of the {001}|{101} facets. (Reprinted with the permission of ref [50] copyrights 2013 © Elsevier). (e) Distribution of electrons and holes on the {001} and {101} facets. (f) DOS of TiO_2 {001} and {101} surfaces. (Reprinted with the permission of ref. [51], copyrights 2011 © John Wiley and Sons).

2.1.3. Optical Properties

Apart from preferential oxidation–reduction ability, the band gap of the TiO_2 nanomaterials would also change according to the arrangements of crystal facets on the surface [52]. Based on X-ray photoelectron spectroscopy (XPS) VB spectra and DFT electronic structure calculations, Liu et al. revealed two significant points: (1) the band gap of {001} facets was smaller than that of {101} facets, and (2) the VB maximum of {001} facets was identical to that of {101} facets and thus the CB minimum of {001} facets was lower than that of {101} facets. (Figure 3d) [53]. Hence, the UV-Visible spectrum of anatase TiO_2 with 72% {101} facets show blue shifts compared to that with 72% of {001} facets. This electronic band difference would certainly affect the photocatalytic activity of the catalysts in the visible light region [54]. However, up to now, no appreciable visible activity has been observed for pure anatase TiO_2 exposed with {001} facets. To make visible light active, these nanomaterials are coupled with other materials.

2.1.4. Photocatalytic Selectivity

The selectivity of the photocatalysts towards pollutants/organics is a very important aspect for its conversion/transformation. The selectivity of the TiO_2 can be enhanced by increasing the percentage of {001} facets on its surface. Li et al. demonstrated that the photocatalytic selectivity for the conversion of toluene to benzaldehyde can be enhanced by increasing the specific surface area of exposed {001} facets. [55]. Similarly, the rate of photoconversion of azo dyes is found to be higher for the TiO_2 -001 materials [56].

This selectivity can be related to the special atomic configuration and associated surface terminating Ti-F bonds which dominates the interaction between {001} facets and certain organic compounds [53]. Ohtani et al. suggested that the acid strength of hydroxyl ions on {001} facets is lower than the {101} facets which is further confirmed by the zeta potential measurement. This difference in the surface charge significantly affects the adsorption properties and photocatalytic conversion of organic pollutants [57].

2.2. Properties of TiO_2 -001 Surfaces for Li-ion Battery

Lithium-ion batteries (LIBs) have been a widely applied system to store electrical energy, for both mobile and stationary applications. TiO_2 -based anodes are the most attractive candidates for building lithium-ion batteries due to the following characteristics: (1) high specific surface area, (2) low volume change during Li ion insertion/desertions process (<4%), which is important for good cycling stability, (3) low internal resistance, (4) low intercalation potential for Li, (5) low price, (6) environmentally friendly, and (7) safe and durable.

Among other forms of TiO_2 , TiO_2 nanosheets with exposed {001} facets offer very high surface areas ($\sim 170 \text{ m}^2 \text{ g}^{-1}$) which provides more lithium insertion channels, and short paths for Li-ion diffusion with high speed, which are crucial for good rate capability (Figure 4). Accordingly, the first discharge capacity of 300 mAh g^{-1} was reported at 0.5 C and a reversible capacity of 150 mAh g^{-1} was achieved at current rate of 10 C for TiO_2 -001 surfaces [58]. Moreover, anatase TiO_2 , having different percentages of (001), demonstrated different behaviors for Li^+ ions insertion. Hengerer et al. showed that the lithium insertion is favored on the (001) surface as compared to 101 surfaces. This can be confirmed by a higher standard rate constant for charge transfer 10^{-8} vs. $2 \times 10^{-9} \text{ cm}^2/\text{s}$ and a higher chemical diffusion coefficient for Li^+ insertion 4×10^{-13} vs. $2 \times 10^{-13} \text{ cm}^2/\text{s}$ [59].

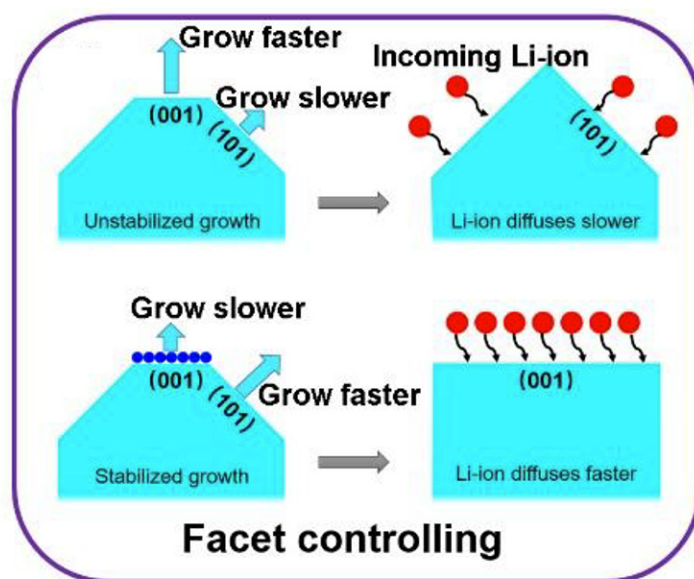


Figure 4. Li-ion insertion on TiO_2 -001 surfaces [60].

Cheng et al. compared the electrochemical properties of 001 TiO₂ nanosheets with the Degussa P25, which can be seen in Figure 5. They revealed that the TiO₂-001 surfaces exhibit an excellent capacity retention at 10 C charge–discharge rate (101.9 mA h g⁻¹ after 100 cycles), and enhanced rate performance at 0.5–10 C current rates as compared with Degussa P25 TiO₂ nanoparticles (NPs) [61].

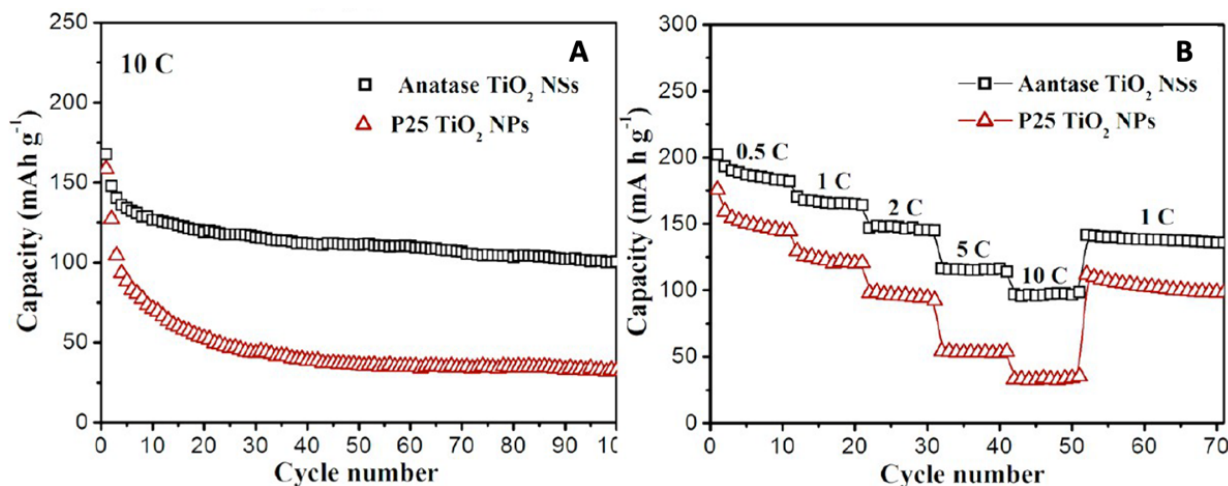


Figure 5. (A) Cycling performances of the anatase TiO₂ NSs and P25 TiO₂ NPs at 10 C. (B) Rate capability of the anatase TiO₂ NSs and P25 TiO₂ NPs at 0.5–10 C. (Reprinted with the permission of ref. [61], copyrights 2014 © American Chemical Society).

The specific capacity and cycling performances can be further enhanced by integrating the advantages of 001 faceted nanosheets and their highly porous organization. Yu et al. demonstrated that the TiO₂ hollow microspheres exhibit numerous active sites and efficient accommodation of volume changes during the charging and discharging process, leading to superior capacity and rate capability. This excellent electrochemical performance can be attributed to the hollow nature and exposed high-energy {001} facets of the 3D assembled electrode structure [20].

2.3. Methods to Modify the Properties of TiO₂-001 Surfaces

The scientists have developed many chemical methods to modify TiO₂ by shifting its optical response to the visible range. Some of them are given in Figure 6.

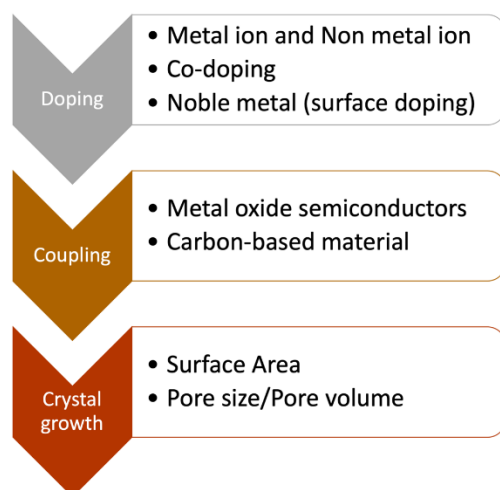


Figure 6. Methods to modify TiO₂-001 nanomaterials.

2.3.1. Doping

One of the most common methods to modify the properties of TiO₂-001 is through doping. Doping intentionally introduces impurities into pure TiO₂-001 semiconductors and can be done for the purpose of modulating its physical, chemical and optical properties [62]. The choice of the dopant is dependent upon its properties, such as ionic radii, conductivity and chemical stability. Here, we will discuss metal and non-metal ion doping [63].

Metal ion doping: Metal ion doping involves a substitution of Ti group by a transition metal or rare earth metal ion [64,65]. Doping with a metal ion increases the formation of Ti³⁺ ions, leading to enhancement in the photocatalytic activity, as more Ti³⁺ states may cause more oxygen defects which facilitate the efficient adsorption of oxygen on the titania surface. The formation of O²⁻ upon chemisorptions of oxygen requires the presence of a surface defect site which can be enhanced by metal ion doping. Since the redox energy states of many metal ions lie within the band gap states of TiO₂, the substitution of metal ions into the TiO₂ introduces an intraband state close to the CB or VB edge, inducing visible light absorption at sub-band gap energies. Zhang et al. and Zhu et al. reported that Mo-doped and La-doped TiO₂-001 showed more enhancement in the photoactivity than the pure TiO₂ [66,67].

Non-metal ion doping: For non-metal doping in TiO₂ in anionic sites (oxygen), wide varieties of anionic species N [68], S [69], C [70], or F [71] have been used. This approach consists of the substitution of a non-metal atom for an oxygen atom in TiO₂. There are three different main opinions regarding modification mechanisms of TiO₂ doped with non-metals.

- (a) **Band gap narrowing:** Dozzi et al. [72] found N 2p state hybrids with O 2p states in anatase TiO₂ doped with nitrogen because their energies are very close, and thus the band gap of N-TiO₂ is narrowed and able to absorb visible light.
- (b) **Impurity energy level:** Yalda et al. [73] stated that TiO₂ oxygen sites substituted by nitrogen atom form isolated impurity energy levels above the valence band irradiation and UV light excites electrons in both the VB and the impurity energy levels, but illumination with visible light only excites electrons in the impurity energy level.
- (c) **Oxygen vacancies:** Gonzalez-Torres et al. [74] concluded that oxygen-deficient sites formed in the grain boundaries are important for the emergence of vis-activity and nitrogen doped into oxygen-deficient sites are important as a blocker for reoxidation.

Codoping: Heterostructuring the TiO₂-001 by codoping with two or more dopants is reported to achieve significant synergistic effects compared to their single ion doped or undoped TiO₂ counterparts [75,76]. The strong interaction between these dopants within the TiO₂ matrix alters the charge carrier transfer-recombination dynamics and shifts the band gap absorption to the visible region [77]. In the case of Ni and N [78], N broadens the absorption profile, improving the photoutilization of TiO₂, and generates more electron-hole pairs, while Ni doping restrains the increase of grain growth and leads to crystal expansion, retarding the recombination of charge carriers and thus resulting in the faster degradation of MO compared with single ion doping or undoped TiO₂ under UV light.

Noble metal ion doping (surface doping): Noble metal doping creates high Schottky barriers in the TiO₂ lattice which acts as electron traps by promoting interfacial electron transfer and thereby suppressing the recombination [79]. Noble metal islands deposited on the TiO₂ surface show surface plasmon resonance (SPR) due to which the visible light absorption of the catalysts increases drastically [80]. It has been reported in the literature that the noble metals such as Pt [81], Au [82] and Pd [83] deposited on TiO₂-001 have high Schottky barriers among the metals and thus act as electron traps and increase visible light absorption through SPR effect.

2.3.2. Coupling

Coupling TiO_2 -001 with carbon-based materials: Carbon-based materials such as carbon nanotubes, carbon quantum dots, fullerenes, graphene, graphene oxide, reduced-graphene oxide and graphene quantum dots have been proven as effective materials to couple with 001- TiO_2 . This coupling further suppresses the recombination of the photogenerated electron–hole pairs. These carbon-based materials have the following characteristics, which make them an ideal candidate for coupling with TiO_2 -001 materials [29].

- High surface area: High specific surface area with many active sites on the surface to boost photocatalytic reactions as compared to their bulk counterpart.
- π -conjugated structures: This leads to fast electron transfer and promote the separation of electron–hole pairs on the photocatalyst surface.
- Excellent support matrix: Carbon-based materials can form efficient heterojunction by having intimate contact between them and TiO_2 -001 materials, such as point-to-face contact (0 D) for carbon/graphene quantum dots, line-to-face contact for carbon nanotubes (1 D) and face-to-face contact for graphene (2 D) as presented in Figure 7. This is more beneficial for the rapid charge transfer and better catalytic dispersion to enhance the photocatalytic activity [84,85].

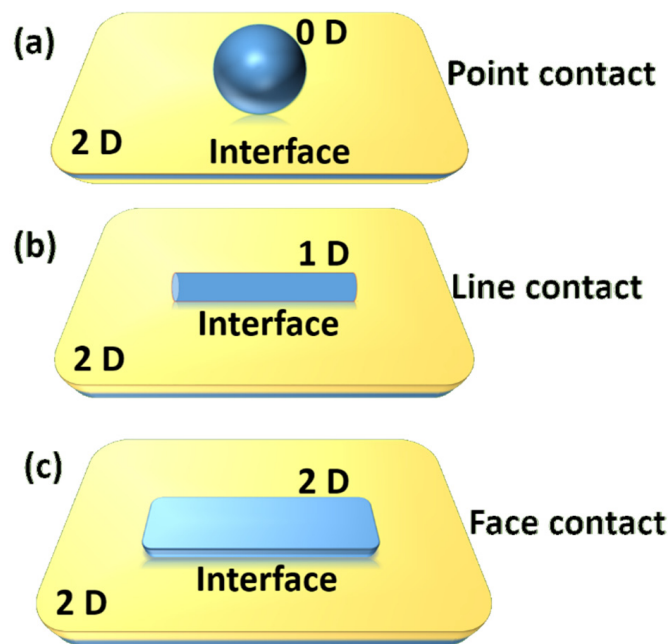


Figure 7. Schematic diagram of interfaces of (a) 0 D (b) 1 D and (c) 2 D materials with TiO_2 -001 nanosheet surfaces [84].

There is a cornucopia of examples that explore carbon-based, material-based nanocomposites which could advance fabrication photocatalysis and Li-ion battery anodes. Some of them are discussed in detail in the application section of this review [31,86–88].

Coupling TiO_2 -001 with other semiconductors: TiO_2 -coupled semiconductor photocatalysts are a novel approach to achieve more efficient charge separation [89]. It increases the lifetime of the charge carriers (as shown in Figure 8), and enhances interfacial charge transfer to adsorbed substrates [90]. At the same time, physical and optical properties of the coupled nanocomposites are greatly modified.

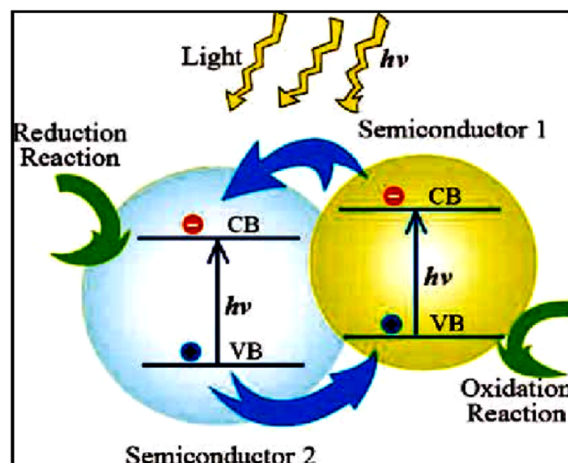


Figure 8. A pictorial representation of the coupling of a semiconductor with TiO₂.

Metal oxides, such as Cu₂O [91], Fe₃O₄ [92], CdS [93], MoO₃ [94], SnO₂ [95], and so on, have been considered for band gap engineering of TiO₂ which are discussed in detail in application section.

Among these oxides, low band gap Cu₂O is used as a sensitizer to enhance visible light absorption [96], whereas other large band gap oxides (SnO₂) are coupled with TiO₂ for extrinsic trapping of photogenerated charge carriers to enhance photoactivity. Coupling TiO₂ with SnO₂ has attracted much attention for Li-ion battery applications, as the theoretical lithium storage capacity is of SnO₂ 790 mAhg⁻¹, which is more than twice that of graphite (370 mA hg⁻¹) [31].

2.3.3. Crystal Growth

During synthesis, the formation of faceted TiO₂ crystals is always influenced by different environmental growth conditions (either acidic or alkaline conditions). By simply manipulating the pH or concentration of the HF solution used, the size, shape and morphology of {001} faceted TiO₂ crystals could be effectively controlled [97,98]. As a result, the morphologies of the as-synthesized anatase vary with surface chemistry and thus the photoactivity [99]. Various morphologies reported for TiO₂-001 are given in Figure 9.

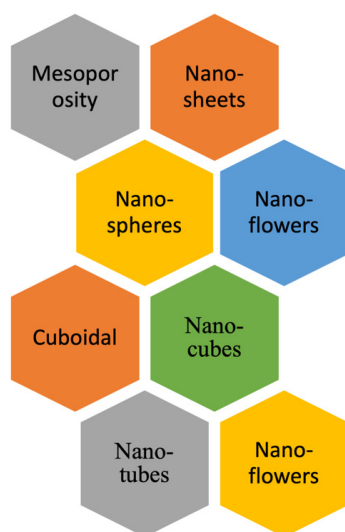


Figure 9. Various morphologies reported for TiO₂-001 structures.

In this case, efforts are being made to synthesize TiO₂-001 with high surface areas and porosity. Two-dimensional structures like nanoplates, nanosheets and hierarchical

structures like nanoflowers provide high surface area and active sites for catalytic adsorption [100]. Porous structures can provide a wide surface area with cavity effect [101,102]. This photon energy entrapment in a porous structure may further expand the photophysical effect in applications, such as photocatalysis and Li-ion batteries [20,103].

3. Synthesis of TiO_2 -001 and TiO_2 -001-Based Composites

According to the Wulff construction, the equilibrium shape of anatase crystals is a slightly truncated bipyramid having eight $\{101\}$ and two $\{001\}$ facets (Figure 10). This is the most popular crystal shape occurring in nature with a typical degree of truncation (B/A) in an order of 0.3–0.4 range, giving less than 10% of $\{001\}$ exposed facets [30].

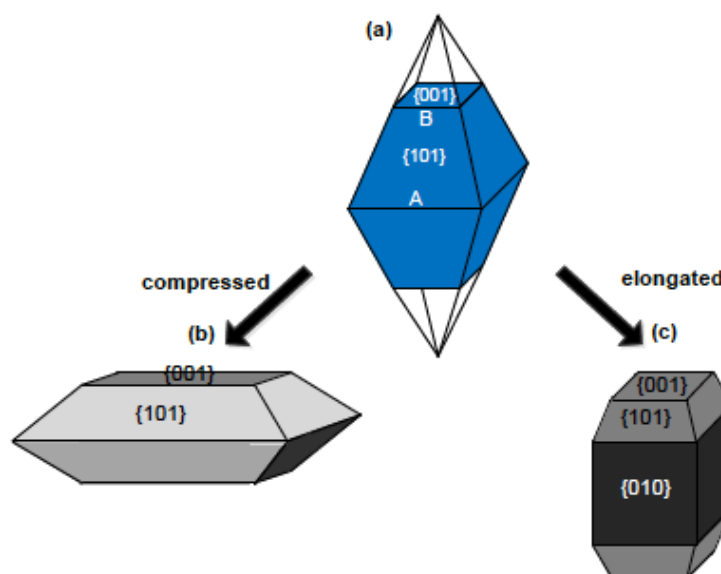


Figure 10. (a) Shape of anatase TiO_2 under equilibrium conditions, (b,c) shape of anatase TiO_2 under non-equilibrium conditions. The side lengths labelled as A and B are used to estimate the degree of truncation (B/A) and also calculate the percentage of exposed $\{001\}$ facets. (Reprinted with the permission of ref. [30], copyright 2014 © John Wiley and Sons).

3.1. Synthesis of TiO_2 -001 Nanomaterials

To synthesize TiO_2 nanocrystals with dominant 001 facets, the crystal growth should be confined within the kinetically controlled regime under non equilibrium conditions [42]. The key in controlling the percentage of any exposed facets is to alter their relative stability during crystal growth, which could be achieved with the help of surface adsorption of capping agents [37]. In short, a general approach to control the percentage of any crystal facets present is to grow the crystal in the presence of a capping agent (adsorbing species) which can alter its surface energy. Thus, the role of capping agents is crucial to selectively adsorb and reduce the surface free energy of materials with more active sites inhibiting the crystal growth along the corresponding direction [104].

To investigate the effects of various adsorbates (capping agents) on the stability of $\{001\}$ facets, Yang et al. systematically explored a range of 12 non-metallic adsorbate atoms X ($X = \text{H, B, C, N, O, F, Si, P, S, Cl, Br}$ and I) by performing first-principles calculations. The calculated surface energies (γ) for all the 12 adsorbates are illustrated in Figure 11a [43].

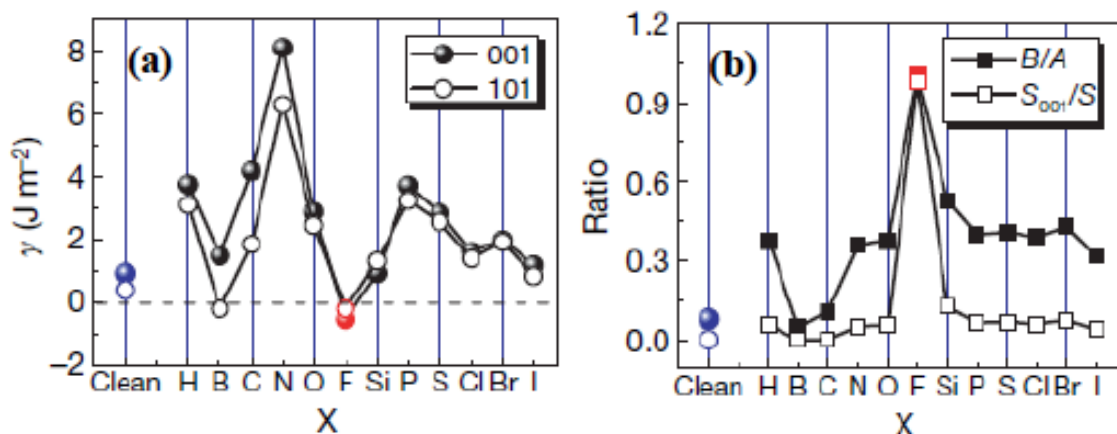


Figure 11. (a) Calculated energies of the {001} and {101} facets surrounded by X atoms (X = H, B, C, N, O, F, Si, P, S, Cl, Br and I). (b) Plots of the optimized value of B/A and percentage of exposed {001} facets for single anatase crystal with various adsorbate atoms X. (Reprinted with permission from ref. [43], Copyright 2008 © Nature Publishing Group).

Referring to Figure 11a, two conclusions were: (1) F-terminated anatase TiO₂ surfaces have the lowest γ for both {001} and {101} facets among the 12 non-metal-terminated surfaces, and (2) {001} facets are preferential and more stable compared to {101} facets for F-terminated anatase TiO₂ crystals. On the basis of these experiments, they verified that there is strong preferential interaction between fluorine and the {001} facets of anatase TiO₂ crystals which enhances the relative stability of the {001} facets during the crystal growth. Hence, they used HF as a capping agent and TiF₄ as raw material in a hydrothermal reaction to synthesize TiO₂-001, which yielded TiO₂ with 47% {001} facets. This breakthrough stimulated many research efforts towards the synthesis of TiO₂-001 with an increased percentage of {001} facets using HF as a capping agent [43].

Along with the HF, Yang and co-workers used 2-propanol to synthesize high quality anatase TiO₂ crystals with 64% of exposed {001} facets. They discovered that alcohols not only acted as a reaction medium, but also as a protecting agent to manipulate the isotropic growth of anatase TiO₂-001 nanomaterial [105,106].

Though there are many investigations into TiO₂-001 synthesis using HF as a capping agent, the use of HF is extremely corrosive. Hence, many researchers are now adopting HF-free synthesis methods which are comparatively safe and environmentally friendly. Some of them are mentioned in Table 1.

Table 1. Fluorine-mediated synthesis routes.

Precursor	Capping Agent	Synthesis Route	Solvent	% Of 001 Facets	Reference
TiF ₄	HF	Hydrothermal	Water	47	[43]
Titanium butoxide	HF	Hydrothermal	Water	89	[107]
TiF ₄	HCl	Hydrothermal	Water	>90	[108]
TiF ₄	Disodium EDTA	Hydrothermal	Water	22.8	[109]
TiCl ₄	NH ₄ F and 2-propanol	Solvothermal	Alcohol/water	-	[110]
TiOSO ₄	NH ₄ HF ₂	Solvothermal	Water	-	[111]
TiCl ₄	NaBF ₄ and NaF	Solvothermal	HCl/water	55%	[112]
(NH ₄) ₂ TiF ₆	H ₃ BO ₃ and 2-propanol	Solvothermal	H ₃ BO ₃ and 2-propanol	-	[113]

However, F-containing compounds generate toxic and corrosive substances at elevated temperatures in hydrothermal synthesis [114]. Moreover, due to the strong interaction between TiO₂-001 crystal surface and F⁻ ions, removing them is very difficult. Thus,

developing a fluorine-free synthesis methodology is very necessary. To date, there are some papers reporting fluorine-free strategies for fabricating anatase TiO₂-001, which are listed in Table 2.

Table 2. Fluorine-free synthesis routes.

Precursor	Capping Agent	Synthesis Route	Solvent	Reference
TiO ₂ powder	Oleic acid Oleyamine	Solvothermal	Water vapor	[115]
Amorphous TiO ₂	Polyvinyl pyrrolidone with acetic acid	Electrospun followed by hydrothermal method	9.6%	[116]
TiCl ₄	Ethylene glycol	Hydrothermal	18%	[117]
K-titanate wires	(NH ₄) ₂ (CO ₃)	Hydrothermal	60%	[114]
Ti-isopropoxide	DETA -and isopropyl alcohol	Solvothermal	~100%	[58]
Tetrabutyl titanate	H ₂ SO ₄	Hydrothermal	~100%	[118]
Ti-isopropoxide	DEA-TBAH	Hydrothermal	-	[119]
Ammonium titanate nanowires	HMTA	Hydrothermal	-	[120]
TiCl ₃	H ₂ O ₂	Hydrothermal	-	[121]

DETA—diethylene triamine; TBAH—tetrabutyl ammonium hydroxide; HMTA—hexamethylene tetraamine.

Among the methods to grow TiO₂-001, the hydrothermal method is more often used, as can be noticed in Tables 1 and 2. Some other methods which can be used are the microwave heating method [13], chemical vapor deposition (CVD) [122] and the electrochemical anodization method [123]. Among these methods, CVD is often used to synthesize high-density TiO₂-001 thin films with preferred orientation. In a recent work, Lee and Sung reported the synthesis of TiO₂ nanosheets on silicon and silicon-coated substrates using the CVD method. They discovered that the silicon vapours can suppress the growth of anatase crystals into [1] orientation, resulting in the formation of 2D-nanosheets with dominant {001} facets [124].

3.2. Synthesis of TiO₂-001-Based Composites

As explained in the previous section, there are several types of TiO₂-001-based composites which mainly include TiO₂-001 doped with metal or non-metal, noble metal deposited TiO₂-001 nanomaterials and TiO₂-001 coupled with other semiconductors or carbon-based materials.

Hydrothermal and solvothermal methods are the most common methods used for the synthesis of doped TiO₂ composites. For doping a particular metal/non-metal ion, a soluble precursor containing that ion is added during the hydrothermal reaction. However, fluorine-rich hydrothermal methods yield products with very high crystallinity, making the inclusion of dopant species into the structural framework difficult [125]. Hence, very specific dopant precursors have to be used for the synthesis of doped TiO₂-001 composites. For example, for nitrogen doping, titanium nitride has been used as both a Ti precursor and an N doping source [68]. TiS₂ and TiC have been used as a sulfur and carbon precursor, respectively [126].

For noble metal deposition, TiO₂-001 is synthesized by a hydrothermal method and noble metal is deposited on it by photochemical or chemical reduction process. In this context, core-shell morphology is highly preferred due to their controllable chemical and colloidal stability within the shell and charge transfer between metal cores and semiconductors [104]. Wu and co-workers successfully fabricated Au/TiO₂-001 nanomaterials in a core-shell form in which TiO₂ nanomaterials have truncated wedge-shaped morphology. A schematic of the synthesis method is shown in Figure 12 [127]. They demonstrated that

the morphological evolution of TiO₂ shells is highly dependent on the concentration of F⁻ ions produced during the reaction. The F⁻ ions play a dual role of producing well-defined wedge-like TiO₂ shells and directing growth of truncated crystal {001} facets.

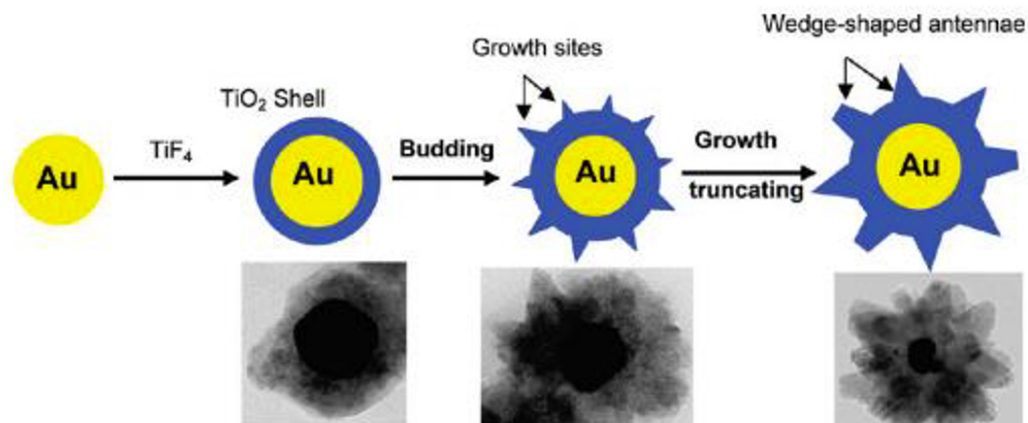


Figure 12. Schematic illustration of the proposed formation process of core-shell Au/TiO₂ nanoparticles with truncated wedge-shaped morphology. (Reprinted with the permission from ref. [127], copyrights 2009 © American Chemical Society).

TiO₂-001 coupled with other semiconductors could also be synthesized by only the hydrothermal method or it can be used in combination with a sol gel and template method or the layer-by-layer (LBL) self-assembly method. Shen et al. developed a magnetic composite consisting of Fe₃O₄/SiO₂/Au/TiO₂ sandwiched layers. A schematic of synthesis is shown in Figure 13. Considering Fe₃O₄ as a core nanomaterial, a SiO₂ layer is deposited on it by sol gel synthesis using ethylene glycol, tetraethyl orthosilicate (TEOS). Then, the Au nanomaterials are coated on this assembly using electrostatic layer-by-layer and interfacial growth methods. Finally, the TiO₂ layer is assembled using the hydrothermal method. This catalyst shows higher photocatalytic activity in visible light and magnetic separability. Moreover, these sandwich-structured photocatalysts can be applied to other catalytic systems such as dye decoloration, water decomposition, hydrogen generation and so on [92].

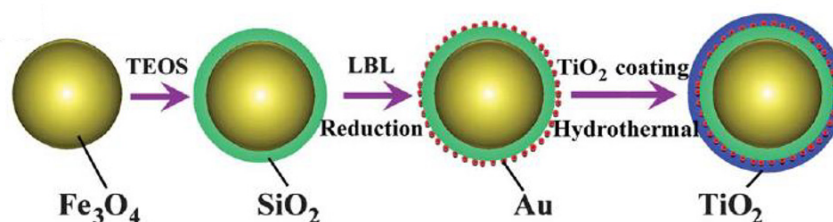


Figure 13. Schematic illustration of the synthetic process of the Fe₃O₄/SiO₂/Au/TiO₂ photocatalysts. (Reprinted with the permission of ref. [92], copyrights 2012 © Royal Society of Chemistry).

Similarly, for the synthesis of TiO₂-001 composites with carbon-based materials, hydrothermal or solvothermal methods have been used extensively. This process is usually followed by microwave heating or ultrasonication for the uniform distribution of TiO₂ materials on graphene template. A schematic of the process is shown in Figure 14 [128].



Figure 14. Schematics for the preparation of graphene/TiO₂ nanocomposites by a hydrothermal treatment in the solvent of ethanol, water and HF. (Reprinted with the permission of ref. [128], copyrights 2012 © Royal Society of Chemistry.

4. Applications

4.1. TiO₂-001-Based Composites for Photocatalytic Applications

Most of the photocatalytic reactions occur on the surface of a photocatalyst and involve the transfer of photogenerated charge carriers. Therefore, the surface electronic structure plays an important role in the photocatalytic activity of TiO₂ nanomaterials. Theoretical predictions suggest that the {001} facet has the highest surface energy and special atomic structure. Hence, {001} faceted TiO₂ nanoparticles show superior performance in photodegradation, water splitting and reduction of CO₂.

Additionally, it is noted that TiO₂ nanosheets with {001} facets can reduce the recombination rate of the photogenerated electron hole pairs. To further increase the charge separation efficiency and visible light absorption ability, TiO₂-001 nanomaterials are coupled with other materials. Recently, various allotropes of carbon materials, including active carbon, carbon nanotubes (CNTs) graphene, graphene oxide (GO) and reduced graphene oxide (rGO) have been combined with TiO₂, opening a door to a research frontier for these new, smart composite materials [87,129]. Among all, graphene is the star material for modifying the properties of the photocatalyst material. Figure 15 displays the major roles of graphene in the resulting composite photocatalysts [29]. It is believed that TiO₂-001-graphene composites are high-performance candidates in photocatalytic applications. Some of these composites and their applications are listed in Table 3.

Table 3. Photocatalytic applications of TiO₂-001-based composites.

Catalysts	% Of 001 Facets	Synthesis Methods (TiO ₂ Composites)	Applications	Ref
TiO ₂ on graphene sheets	61	Fluorine-mediated microwave-hydrothermal (ethanol-water)	H ₂ production	[130]
TiO ₂ on graphene sheets	64	Fluorine-mediated solvothermal method	Degradation of RhB	[131]
Graphene-TiO ₂ composites	~100%	Fluorine-mediated solvothermal method	Degradation of methylene blue	[132]
Graphene-TiO ₂	-	Flurine-mediated solvothermal (methnol-water)	H ₂ production	[133]
Graphene-TiO ₂	-	Solvothermal method without any capping agent	Degradation of methylene blue	[28]

Table 3. Cont.

Catalysts	% Of 001 Facets	Synthesis Methods (TiO ₂ Composites)	Applications	Ref
Graphene aerogels–TiO ₂	50%	Glucose-mediated hydrothermal method	Degradation of methyl orange	[134]
Graphene foam–TiO ₂	-	Fluorine-mediated solvothermal method (ethanol–water)	Degradation of Cr (IV), methyl orange and phenol	[135]
RGO–TiO ₂	-	Fluorine-mediated solvothermal method	Degradation of basic violet	[136]
RGO–TiO ₂	-	(DETA)-mediated by solvothermal method	Photo-electrochemical current	[137]
Carbon dots–TiO ₂	-	Fluorine-mediated hydrothermal method	H ₂ production	[138]
Carbon fibres–TiO ₂	40–92	Fluorine-mediated hydrothermal method	Degradation of methyl orange	[139]
Mesoporous-carbon nitride C ₃ N ₄ -TiO ₂	80.6	TiO ₂ fluorine-mediated hydrothermal, composite-mechanical stirring	Degradation of methylene blue	[140]
CNTs–TiO ₂	75%	Fluorine-mediated hydrothermal method	Degradation of RhB	[141]
Fe ₃ O ₄ @TiO ₂ core-shell	-	Combination of template and solvothermal method	Degradation of methylene blue	[142]
SrTiO ₃ -TiO ₂	-	Fluorine-mediated hydrothermal method	Degradation of RhB dye	[143]
Bi ₄ O ₅ Br ₂ -TiO ₂	-	TiO ₂ : Fluorine-mediated hydrothermal method Composite: Electrostatic self-assembly	NO removal	[144]
Au/TiO ₂	58–77	TiO ₂ : Fluorine-mediated hydrothermal method Au photodeposition: green method using citrate ions	Photocurrent density	[82]
Pt/TiO ₂	75	TiO ₂ : Fluorine-mediated hydrothermal method Pt deposition: Photochemical reduction	Hydrogen Production	[81]
PdO–TiO ₂	-	TiO ₂ : Fluorine-mediated hydrothermal method PdO deposition: Wet impregnation	Degradation of methylene blue and photocurrent measurement	[83]
Carbon nitrides–TiO ₂	-	Fluorine-mediated hydrothermal method	Photoreduction of CO ₂ to CO	[145]
Polymer–TiO ₂ –Graphene	-	Sonochemically assisted fluorine mediated solvothermal method	Photoreduction of CO ₂ to CO	[146]
N-doped TiO ₂ –graphene	-	Fluorine-mediated solvothermal method	Photoreduction of CO ₂ to CH ₄	[147]

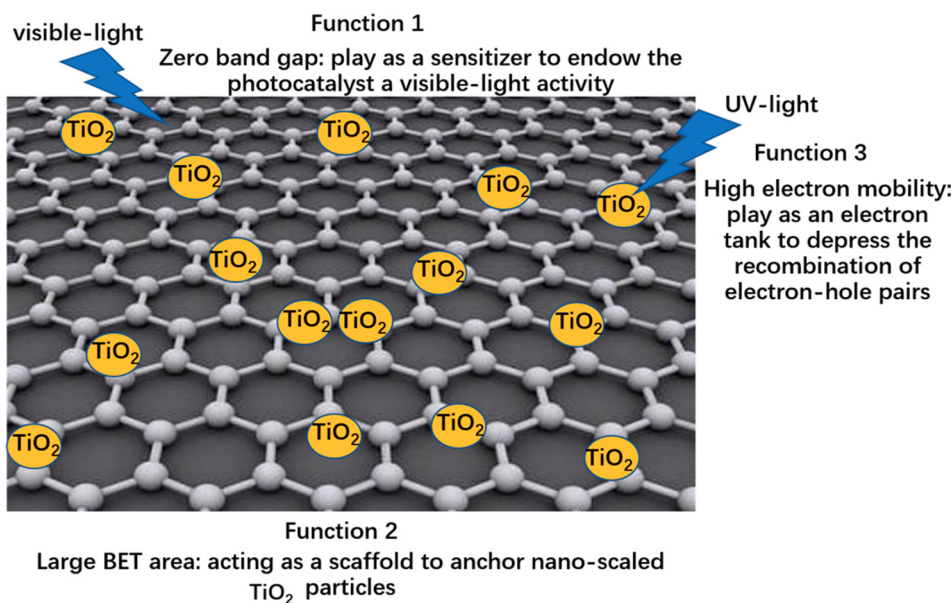


Figure 15. Role of graphene in TiO₂-001–graphene composites [29].

Xiang et al. deposited hydrothermally synthesized TiO₂ nanosheets with exposed {001} facets on graphene sheets by the microwave method. Among all the composites with 0.2 to 5% graphene content, 1% showed almost 41-times higher photoactivity than the pure TiO₂. In the composite material, graphene can act as an efficient charge separator due to the ideal heterojunction formed between the graphene and TiO₂ nanomaterials. As can be seen from the band diagram of TiO₂ and graphene, the valence band of graphene lies below (−0.24 V) the conduction band of anatase TiO₂ (Figure 16) [148] which favors the electron transfer from the conduction band (CB) of TiO₂ to graphene sheets. Furthermore, the lower potential value of valence band of graphene is 0.08 V, which is slightly higher than the reduction potential of H⁺ (0 V), which favors the reduction H⁺ to H₂, thus enhancing photocatalytic H₂-production activity [130].

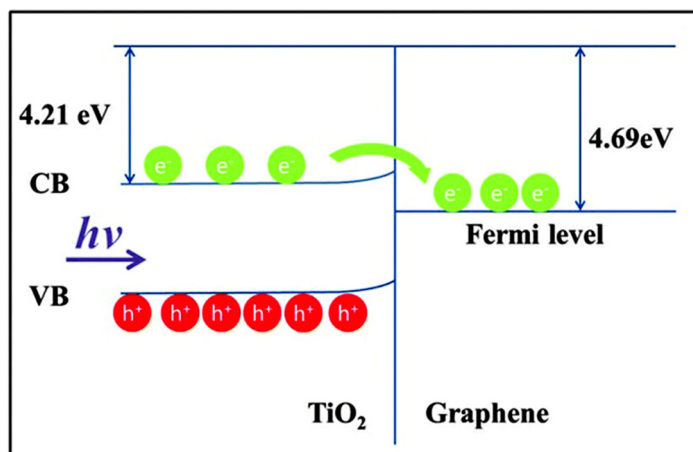


Figure 16. Band diagram of TiO₂ and graphene heterojunction [148].

Similarly, Sun et al. fabricated nano-sized anatase TiO₂-001 nanosheets by the solvothermal route using HF as the morphology controlling agent. These nanosheets were deposited on graphene sheets by the molecular grafting method. These photocatalysts show 2.8-times enhancement in the photoactivity compared to commercial TiO₂ photocatalysts, which is attributed to the effective charge separation of graphene and the high catalytic activity of {001} facets [131]. Wang et al. demonstrated that the 001 faceted

TiO₂-graphene composites show higher photocatalytic activity than the Degussa TiO₂ for methylene blue degradation reaction. The enhancement in the photoactivity can be attributed to the electron transfer via Ti–O–C between TiO₂ and C interaction which greatly retards the recombination of photoinduced charge carriers. The optimum amount of graphene is found to be 1 wt %, at which the TiO₂/graphene sample displays the highest reactivity [132].

Despite higher photocatalytic efficiency, the biggest problem hindering the applications of TiO₂-graphene composites is their stability. Generally, it is observed that the forces of interaction between TiO₂ and graphene are weak. If the interaction is weak, the composite formation turns out to be inefficient, hampering the transfer of electrons and Li-ions. To avoid this problem, Qiu et al. developed ultralight 3D-graphene aerogels (GAs) which have high surface area, massive appearance and hydrophobic properties. TiO₂ crystals with 001 facets show more stable and higher dispersions on these Gas, which contributes towards the recyclability of these photocatalysts. In this method, glucose is used as a linker and dispersant between TiO₂ and GAs. The strong interaction between TiO₂ and GAs, the facet characteristics, the high electrical conductivity and the three-dimensional hierarchically porous structure of these composites results in highly efficient charge separation and high surface area, showing enhanced photoactivity. In addition to this, these aerogels can better adsorb organic pollutants and can provide multidimensional electron transport pathways, implying a significant potential application for photocatalysis [134].

On similar grounds, Chen et al. developed free standing, 3D graphene foam through leavening GO films. Then, 001 faceted TiO₂ arrays are integrated into these graphene structures through a facile vacuum filtration process combined with a solvothermal method (Figure 17). This results in the uniform distribution of TiO₂ nanosheet arrays into interlayers of graphene foam, forming a 3D hierarchical porous structure. These structures show superior photoactivity towards MO dye degradation, which is 8.7-times higher than the commercial catalysts, i.e., P25. Moreover, these composites are very stable, recyclable and can be reused after 12 runs with high efficiency. The unsaturated coordination atoms and dangling bonds that existed on {001} facets of TiO₂/graphene foam were highly reactive for adsorbing active oxygen species and facilitated the surface catalytic reaction by providing abundant reactive sites [135]. Hence, these composites are highly appreciated for their higher photoactivity, easy separation and reusability.

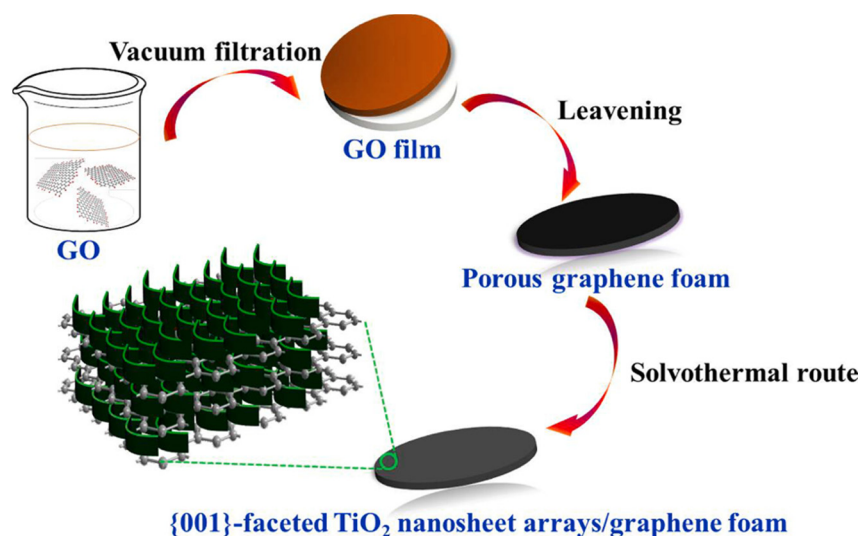


Figure 17. Synthesis route for TiO₂-001-graphene foam composite. (Reprinted with the permission of ref. [135], copyrights 2021© Elsevier).

Graphene oxide (GO) has a similar hexagonal carbon structure to graphene but it also contains hydroxyl (–OH), alkoxy (C–O–C), carbonyl (C=O), carboxylic acid (–COOH) and

other oxygen-based functional groups. GO can be treated by several methods to synthesize reduced graphene oxide (rGO or RGO) in efforts to minimize the number of oxygen groups and achieve properties closer to those of pristine graphene. Liu et al. incorporated rGO into 001 faceted flower-like TiO₂ via solvothermal method. The results indicated that the photocatalytic activities of these composites were significantly improved following the incorporation of RGO, particularly under visible light irradiation [136]. Thien et al. fabricated TiO₂ with highly exposed {001} facets decorated on reduced graphene oxide (RGO) sheets by simple solvothermal route. These composites were sintered at 300, 400 and 500 °C. The results indicated that the composites showed highest photocurrent densities at 500 °C, which is attributed to the reduced recombination of electron–hole pairs and improved light harvesting efficiency [137].

Along with graphene and rGO, other carbon-based materials such as carbon dots and carbon nanotubes can also be coupled with the 001 faceted TiO₂ for higher photoactivities. Sui et al. fabricated carbon quantum dot–TiO₂ composites and Wang et al. prepared carbon nanotubes–TiO₂ composites by a fluorine-mediated hydrothermal method [138,141]. Both composites show higher photocatalytic activity than the pure TiO₂ nanomaterials. Guo et al. introduced carbon fibers (CF), which are flexible, conductive and stable substrate to grow 001 faceted TiO₂ nanosheets [139]. These TiO₂-001/CF hybrid structures exhibited 3.38-fold improved photocatalytic degradation of methyl orange (MO) than commercial catalysts and showed excellent stability under ultraviolet–visible (UV–vis) light irradiation. Graphitic carbon nitride (g-C₃N₄), with a layered structure, is the new class of materials having properties like graphene. It is a polymeric semiconductor consisting of C, N and some impure H, connected via tris-triazine-based building blocks. Due to the presence of N and H atoms it has a basic tendency of H-bonding. Due to its electron-rich properties, it has a capacity to complement carbon in various photochemical applications [149]. Liu et al. developed a (g-C₃N₄- TiO₂-001) photocatalyst via a facile ultrasonic dispersion method. All these composites show higher photocatalytic activities which could be attributed to the synergistic effect of TiO₂ and C, which greatly retard the recombination of photoinduced electrons and holes. Furthermore, the carbon-based materials serve as a photosensitizer and sensitize TiO₂-001 through the newly formed Ti–O–C bond, leading to superior photocatalytic activity [140].

Chen et al. fabricated hollow ellipsoidal structures made up of three-layered structures which act as efficient photocatalysts with magnetic separability. In this complex, hematite (α-Fe₂O₃) nanospindles act as the starting templates, on which the silica (SiO₂) layer is coated by a hydrothermal process. Finally, ultrathin anatase TiO₂ nanosheets (NSs) with exposed (001) facets are deposited on this assembly by the solvothermal process, which acts as a shell. The middle SiO₂ layer is then removed by HF treatment, creating hollow ellipsoidal complex structures. The in situ reduction of α-Fe₂O₃ to Fe₃O₄ imparts magnetic functionality to these photocatalysts, making them magnetically separable under the influence of an applied magnetic field. A schematic of the formation of these three types of structures are shown in Figure 18 [142].

Yue et al. developed SrTiO₃/TiO₂ heterostructure nanosheets with exposed (0 0 1) facets by in situ hydrothermal reaction. SrTiO₃ is a well-known cubic-perovskite-type photocatalyst with a band gap of 3.2 eV and possesses superior chemical stability. As can be seen from Figure 19, the conduction band SrTiO₃ lies 200 mV above the conduction band of TiO₂. This favours the electron transfer from SrTiO₃ to TiO₂, leading to the efficient charge separation. Hence, coupling SrTiO₃ to TiO₂ improves the photocatalytic performances of TiO₂ [143].

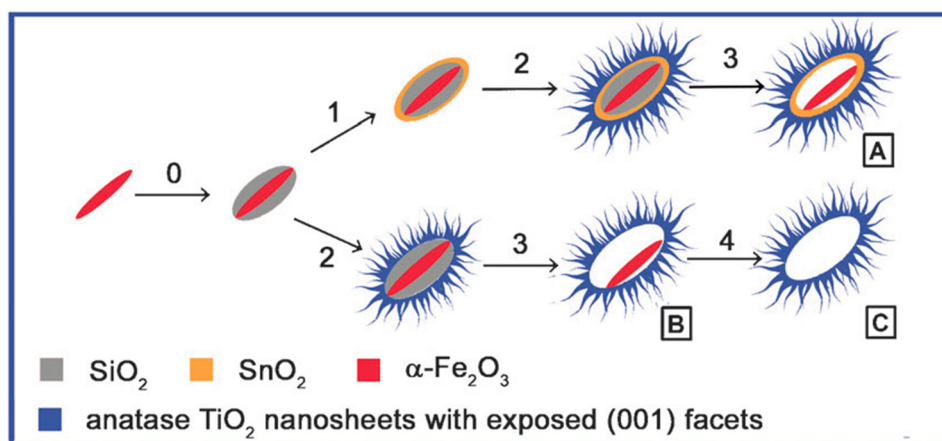


Figure 18. Schematic illustration of the fabrication of the three types of complex hollow structures with various procedures: (0) silica coating on $\alpha\text{-Fe}_2\text{O}_3$ spindles; (1) hydrothermal deposition of SnO_2 layer; (2) solvothermal formation of anatase TiO_2 shell with exposed (001) facets; (3) dissolution of SiO_2 using 0.6% HF; (4) removal of $\alpha\text{-Fe}_2\text{O}_3$ spindle using 0.5 M oxalic acid. (Reprinted with the permission of ref. [142], copyrights 2011 © Royal Society of Chemistry).

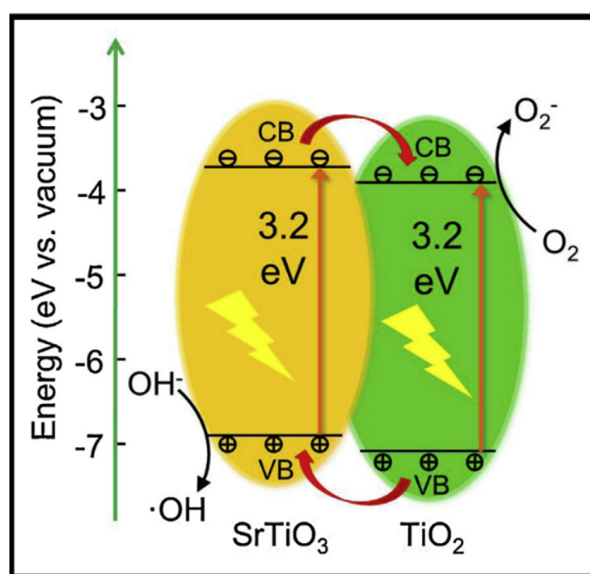


Figure 19. Band diagram of $\text{TiO}_2\text{-SrTiO}_3$ heterojunction. (Reprinted with the permission of ref. [143], copyrights 2014 © Elsevier).

Recently, deposition of noble metals such as Au, Ag and Pt on the surface of semiconductors has been recognized as a promising strategy to achieve visible light harvesting through localized surface plasmon resonance (LSPR) photosensitization. The electrons in noble metals might be excited by the LSPR with visible light absorption and subsequently transfer to the conduction band of the attached TiO_2 semiconductors, increasing the photocatalytic efficiency. Yan et al. fabricated Au-deposited 001 faceted TiO_2 using a green photodeposition method. The close contact between the Au and anatase {001} facet leads to enhanced LSPR intensity and promotes the separation of photogenerated electron–hole pairs under visible light irradiation. This increases the photocatalytic activity of the composites in both hydrogen evolution and methylene blue decomposition [82]. Yu et al. developed Pt/ TiO_2 nanosheets with exposed (001) facets by a hydrothermal route followed by a photochemical reduction deposition of Pt nanoparticles on TiO_2 nanosheets. These composites showed higher photoactivities than the commercial photocatalysts which

can be attributed to the plasmonic effect of Pt nanoparticles and synergistic effect of surface fluorination and exposed (001) facets [81]. Lyu et al. explained that the fluorinated 001 surfaces are controversial to the photocatalytic activities. Hence, they removed the surface F atoms bonding with Ti by the hydrogenation method successfully and found that {001} facet dominant TiO₂ nanosheets without the terminated F atoms showed dramatic enhancement in the photocatalytic activity. Moreover, the clean (001) surfaces are better for PdO deposition than the fluorine rich surfaces. The PdO attached on {001} facets promoted the separation of charge carriers, and Pd nanoparticles transferred plasmonic-induced electrons to the conduction band of hydrogenated TiO₂ under simulated solar irradiation, thus significantly enhancing the photocatalytic activity of Pd-H-TiO₂ composites [83].

To address the serious issue of global warming, TiO₂-001-based composites have gained considerable attention and much research interest for their advancement of converting CO₂ into energy-bearing products without further increasing the concentration of atmospheric CO₂. Crake et al. and Wang et al. synthesized carbon nitrides and graphene composites with TiO₂-001, which show significant photoactivity for CO₂ reduction [145,146].

4.2. TiO₂-001-Based Composites as a Li-ion Battery Anode Material

Li-ion batteries (LIBs) have aided the electronics revolution by powering portable electronics, mobiles and laptops. They have a potential to transform the transportation sector with electric cars, buses and bikes [150,151]. In addition, Li-ion batteries can also be employed to buffer the intermittent and fluctuating green energy supply from renewable resources, such as solar and wind, to smooth the difference between energy supply and demand [152]. These are one of the most advanced rechargeable batteries, which are lighter in weight, smaller in size and have higher energy density as compared to the traditional rechargeable batteries such as lead acid and Ni-Cd [153]. Li-ion batteries operate by shuttling Li⁺ and electrons between negative and positive electrode host structures, which are separated by a separator filled with an aprotic electrolyte. In general, the commercial lithium-ion batteries use a graphite–lithium composite, Li_xC₆, as the anode, lithium cobalt oxide, LiCoO₂, as the cathode and a lithium-ion conducting electrolyte. When the cell is charged, lithium is extracted from the cathode and inserted at the anode. On discharge, the lithium ions are released by the anode and taken up again by the cathode (Figure 20) [154].

To enhance and optimize the electrochemical properties, intense research has focused on all aspects of these batteries, including improved anodes [155], cathodes [156] and electrolytes [157,158]. A wide range of nanostructured materials have been used as a promising electrode material for high-performance LIBs. TiO₂ is a widely studied metal oxide serving as the anode material for LIBs [159–161]. Its most significant advantage is the ability to be charged and discharged at a high current rate (high power). However, TiO₂ has a theoretical lithium storage capacity (170 mA h g⁻¹) which is lower than that of graphite and very poor electronic conductivity. Hence, proper nanostructure engineering is desired to achieve the highly efficient solid-state diffusion of Li⁺ ions from TiO₂ anodes [162]. Fortunately, the recently discovered anatase TiO₂ nanosheets (NSs) with exposed (001) high-energy facets demonstrate high conductivity due to the shorter ion diffusion length (Figure 21) [163]. According to the literature, the energy barrier of Li⁺ entering the (001) surface of anatase TiO₂ is the lowest as compared to the (010) and (101) facets, suggesting much easier migration of Li⁺ across the (001) surface [164]. Hence, these nanosheets also appear to be effective in improving the lithium storage capacity of TiO₂. In addition, 2D TiO₂ nanosheets with a high specific surface area can increase the active sites for Li⁺ insertion, improving its Li⁺ storage capability.

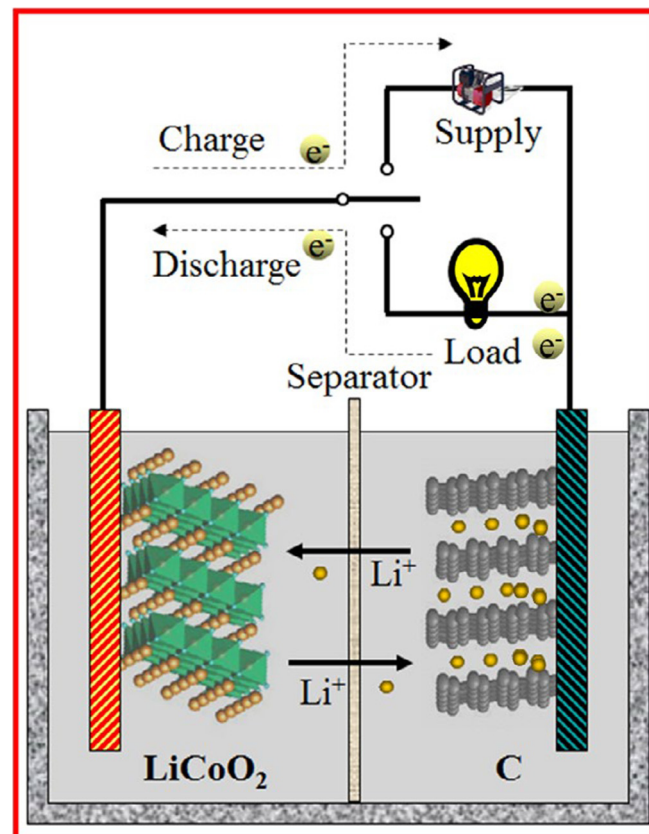


Figure 20. Illustration to show the basic components and operation principle of a Li-ion cell [154].

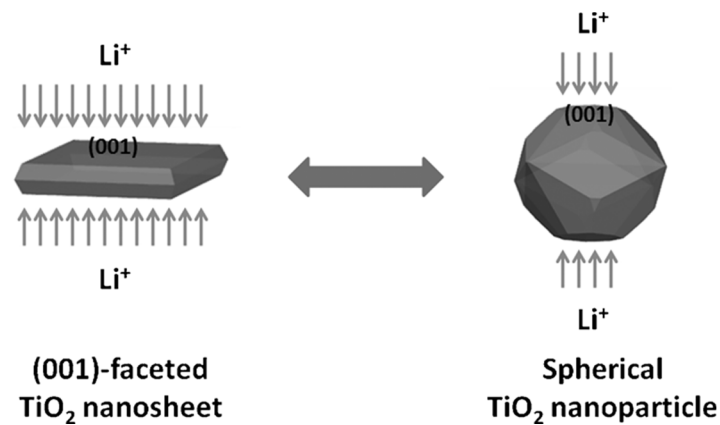


Figure 21. Schematic illustration of the facilitation of lithium diffusion in (001) faceted TiO_2 nanosheets over spherical TiO_2 nanoparticles. (Reprinted with the permission of ref. [163], copyrights 2014 © John Wiley and Sons).

The 2D (001) faceted TiO_2 nanosheets are therefore quite promising as anode materials for design of supercapacitor-like LIBs with high energy and power densities. However, the high energy of the (001) facets results in tight aggregation of the TiO_2 nanosheets when fabricating the anodes. This reduces the access of Li^+ to the active (001) facets and impedes electrolyte penetration inside the structure, deteriorating the electrochemical performances [159]. Hence, TiO_2 -001 nanomaterials are often coupled with other suitable semiconductors to obtain outstanding conductivity and good structure flexibility. Some of the TiO_2 -001-based composites are enlisted in Table 4.

Table 4. Li-ion battery applications of TiO₂-001-based composites.

Catalysts	Synthesis Method	Capacity at Rate (mAh g ⁻¹)	Cycling Performance (mAh g ⁻¹)	Ref
Graphene–TiO ₂ -sandwiched structure	Ionic liquid-mediated solvothermal method	321/1 C	155 at 10 C	[165]
Graphene aerogels–TiO ₂	Glucose-mediated hydrothermal method	605/0.59 C	50 cycles at 0.59 C	[134]
rGO–TiO ₂ hybrid	Fluorine-mediated hydrothermal method	250/1 C	160, 500 cycles at 10 C	[162]
TiO ₂ @graphene nanosheets	Wet chemical method	306	400 cycles	[166]
rGO@TiO ₂ nanotubes	Electrostatic interaction and high temp reduction	263/0.5 C	500 cycles at 0.5 C	[167]
SnO ₂ @TiO ₂	Nanotemplate method	264.8/1 C	100 cycles at 10 C	[168]
MoO ₃ –rutile TiO ₂	Fluorine-mediated hydrothermal method	330/2 C	100 cycles at 10 C	[169]
TiO ₂ –NSs@CNT:	DETA-mediated hydrothermal synthesis	395/1 C	120 cycles at 1C	[170]
Cu–TiO ₂ (001) interface	Fluorine-mediated hydrothermal method	168/1 C		[171]
Carbon supported TiO ₂	DETA-mediated solvothermal synthesis	172.6/1 C	100 cycles at 1 C	[172]

1 C = 335 mA g⁻¹, diethylenetriamine DETA.

The performance of anodes in Li-ion batteries can be evaluated by a number of parameters, such as specific energy, specific capacity, cyclability and the dis/charging rate. Specific energy (Wh/kg) measures the amount of energy that can be stored and released per unit mass of the battery. It can be obtained by multiplying the specific capacity (Ah/kg) with operating battery voltage (V). Specific capacity measures the amount of charge that can be reversibly stored per unit mass. It is closely related to the number of electrons released from electrochemical reactions and the atomic weight of the host. Cyclability measures the reversibility of the Li-ion insertion and extraction processes, in terms of the number of charge and discharge cycles before the battery loses energy significantly or can no longer sustain function of the device it powers. The rate of charge or discharge measures how fast the battery can be charged and discharged, typically called C-rate. At 1C, the battery is fully discharged, releasing maximum capacity in 1 h.

Among all composites, carbon materials, having high electrical conductivity, large surface area, good structural flexibility and modifiable surface functional groups, have been promising as multifunctional substrates to promote the electrochemical performance of TiO₂-001. Liu et al. inserted carbon pillars between TiO₂-001 layers. Such a special structure provides open channels for fast Li-ion insertion and extraction. As a result, these composites demonstrate superior Li-ion storage properties and very high reversible capacities at a current rate as high as 50 C [165]. Yu et al. reported the unprecedented lithium storage and electrochemical performance of hierarchically porous TiO₂-001/rGO hybrid architecture. They discovered that the tightly packed TiO₂-001 nanosheets prevent the insertion of Li⁺/Insertion of rGO prevents aggregation and provides many pathways for the electronic Li ion transport. Moreover, (001) faceted TiO₂ nanosheets grown in situ on the rGO surface show good mechanical stability, specific surface area and high electron conductivity [162]. Qiu et al. fabricated graphene aerogels (GAs)–TiO₂ nanocomposites by a one-step hydrothermal method using glucose as a linker between the two materials (described sect). This TiO₂/GAs anode delivers a high capacity of 605 mAhg⁻¹ in the first discharge which is much higher than other reported TiO₂/carbon electrodes. GAs represent a 3D structured matrix with a large surface area which enhances the dispersion of TiO₂ on GAs. Furthermore, their mesoporosity induces shorter diffusion length for Li-ion insertion and extraction, showing magnificent battery performance [134]. Zheng et al. developed TiO₂-001 nanotubes wrapped with rGO materials. They deposited a GO layer on TiO₂-001

nanotubes by electrostatic interactions and annealed this composite at 700 °C under a 5% H₂/Ar mixed atmosphere. During the annealing process, graphene oxide is reduced to graphene and strongly deposited onto the surface of the TiO₂ nanotubes. At the same time, the mechanically robust 3D matrix can also effectively buffer the large volume change of the active material. Moreover, Ti³⁺ generated during this process increases the electronic conductivity of the composites. The closely coated rGO layer on the nanotube plays a key role in this preservation of morphology, providing a frame for the tube and preventing the TiO₂ from undergoing a phase transformation and breaking into nanoparticles. Because of the advantageous properties of rGO and Ti³⁺, Li⁺ ions can rapidly diffuse into the electrode via the inner space and the thin walls of the nanotubes. Thus, rGO/TiO₂-7ArH exhibits excellent performance as an anode for LIBs [167].

Like graphene, TiO₂-001 nanosheets (NSs) can also be grown on CNTs. The role of CNTs in these composite materials is quite well acknowledged, that is, to form a 3D matrix with superior electronic conductivity. At the same time, the mechanically robust 3D matrix can also effectively buffer the large volume change of the active material. The NSs are uniformly grown on the surface of the CNT backbone along its longitudinal axis. Such a unique CNT-TiO₂-001 NSs nanocomposite shows good capacity retention and high reversible capacities at high current rates of 5 C and 10 C, proving the positive effect of the CNT backbone [170].

Along with the carbonaceous materials, TiO₂-001 coupled with other semiconductors such as SnO₂ and MoO₃ for better electrochemical performance. Chen et al. fabricated TiO₂-001@SnO₂ as a core-shell like structure where SnO₂ materials act as a template for TiO₂ nanomaterial growth (Figure 22B). These ring-like SnO₂ materials encapsulate the SiO₂ core, which can be seen in Figure 22C. Hence, the SnO₂ material acts as a middle layer between the TiO₂-001 shell and SiO₂ core. Afterward, the SiO₂ core is removed by HF treatment, which creates large internal voids inside the TiO₂-001@SnO₂ composites which can be seen in Figure 22E,F. These hollow structures provide extra space which helps to sustain the volume changes during the Li-ion insertion and removal process. These composites showed excellent performance in a Li-ion battery which can be attributed to the TiO₂-001 shell which allows fast transport of Li-ions and large surface area offered by the hollow structures, providing space for Li-ions charge–discharge cycles [168].

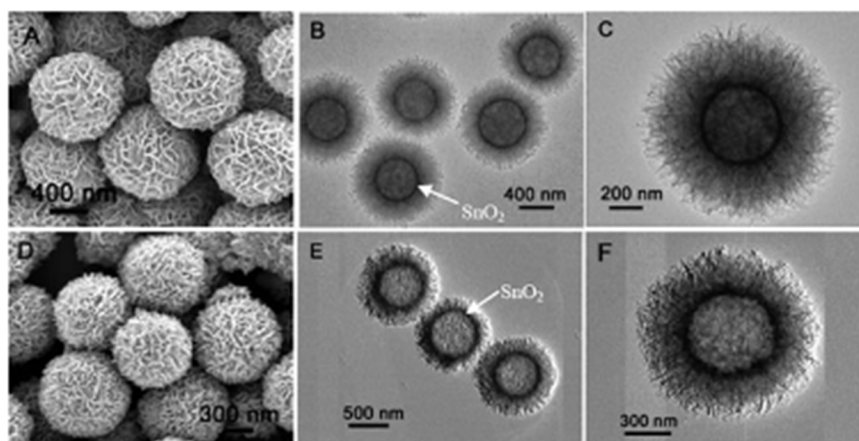


Figure 22. (A) FESEM image and (B,C) TEM images of TiO₂-001 shells grown on SnO₂@SiO₂ core-shell particles. (D) FESEM image and (E,F) TEM images of TiO₂-001@SnO₂ double-shelled hollow spheres. (Reprinted with the permission of ref. [168], copyrights 2010 © Royal Society of Chemistry).

Besides anatase, Chen et al. developed rutile TiO₂-001 nanosheets by a unique hydrothermal method, which forms hierarchical microspheres that closely resemble the natural “desert rose” (Figure 23). These nanocomposites are further coupled with the MoO₃ to form TiO₂-MoO₃ hybrid structures. These hierarchical structures provide high surface area for the uniform dispersion of MoO₃ on the high-energy (001) facets of rutile

TiO₂. In addition, MoO₃ nanomaterials provide sufficient stability to preserve the large number of (001) facets, which significantly improves the Li-ion storage performance of the device [169].

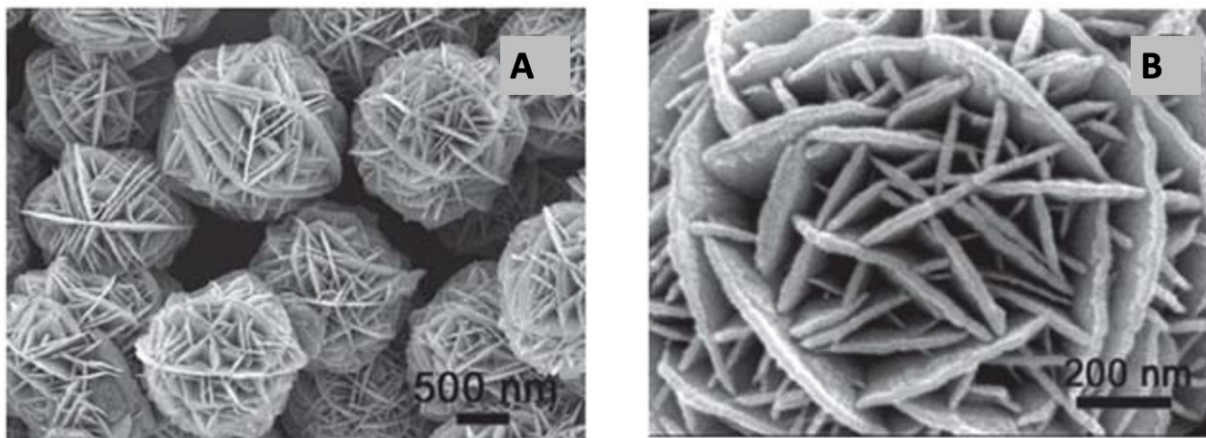


Figure 23. (A,B) Field-emission scanning electron microscopy (FESEM) images of rutile TiO₂-001 nanosheets (desert rose morphology). (Reprinted with the permission of ref. [169] copyrights 2011 © Royal Society of Chemistry).

Liu et al. contacted the single TiO₂ particle with (010) and (001) facets with the two tungsten probes in a scanning electron microscope and found out that the conduction along the [1] direction is an order of magnitude higher than that along the [10] direction. Based on this finding, a TiO₂ anode supported on a copper foil, with its TiO₂ (001)–copper interface similar to the TiO₂ (001)–tungsten interface, was constructed. This shows a remarkably higher lithium storage capability than a reference TiO₂ anode with its interface mimicking the TiO₂ (010)–tungsten interface [171].

5. Conclusions and Future Scope

Intensive research efforts on TiO₂-001-based materials, for their application in environmental remediation and energy conversion, have taken place over the last few years. The continuous advancement in the synthesis methods and modification techniques of TiO₂-001 materials have expanded the capabilities of TiO₂ to include visible light absorption, suppressed rate of recombination, higher electronic conductivity and higher surface area with more active sites. This expands the possibilities of TiO₂ applications into new and diverse areas. Despite the huge development in theoretical studies and experimental investigations involving TiO₂-001 and their composites, practical applications in this field are still in the preliminary stages and many challenges exist in several aspects. Some of the challenges are listed below.

1. Developing novel, large-scale synthesis methods

Despite the great success that has been obtained in the controllable synthesis of TiO₂-001, there is still room for improvement in terms of quality of the products. Most of the synthesis methods employ fluorine-containing solutions as capping agents, which are highly toxic and corrosive. Hence, fluorine-free, safe and environmentally friendly strategies should be developed to obtain clean 001 facets. Moreover, the large-scale and high-yield production methods must be developed, which is an important prerequisite for practical applications.

2. Coupling TiO₂-001 with energy-harvesting materials

The photocatalytic properties of TiO₂-001 materials can be amended by the interaction with new materials, which include light harvesters, charge transport materials, additives and interfacial modifiers. Moreover, many efforts must be made to develop large-scale

preparation techniques for high-quality modified TiO₂-001 materials i.e., TiO₂-001-based composite materials.

3. Exploring new characterization techniques

Scanning electron microscopy (SEM) and transmission electron microscopy (TEM), as well as small-angle X-ray/neutron scattering (SANS/SAXS), are the widely used techniques to investigate the morphologies of {001} and {101} faceted anatase TiO₂ nanocrystals. However, these techniques can only provide selected local morphology information. Moreover, these techniques failed to probe the evolution of TiO₂ surface/interface structures in working conditions, which is crucial to study the complex phase transformation and device stability. Hence, more powerful techniques such as near edge X-ray absorption fine structure (NEXAFS) spectroscopy and neutron pair distribution function (PDF) should be used to obtain accurate average morphology and atomistic structures of {001} and {101} faceted anatase TiO₂ nanocrystals. Moreover, in situ characterization techniques must be developed to reveal the photocatalysis reaction process.

4. Theoretical study for understanding photocatalysis mechanisms

The knowledge about the relationship between the dominant 001 facets and their photocatalytic performance and the reaction mechanism needs to be deepened, especially at the molecular level.

Overall, we believe that future research efforts and developments can benefit TiO₂-001 composites as a next generation material for energy conversion and environmental remediation.

Author Contributions: Conceptualization, A.B. and F.E.; methodology, A.B.; software, F.E.; writing—original draft preparation, A.B.; writing—review and editing, F.E.; visualization, A.B.; supervision, F.E.; project administration, F.E.; funding acquisition, F.E. Both authors have read and agreed to the published version of the manuscript.

Funding: This research received no external funding.

Institutional Review Board Statement: Not applicable.

Informed Consent Statement: Not applicable.

Data Availability Statement: Not applicable.

Conflicts of Interest: The authors declare no conflict of interest.

References

1. Kalair, A.; Abas, N.; Saleem, M.S.; Kalair, A.R.; Khan, N. Role of energy storage systems in energy transition from fossil fuels to renewables. *Energy Storage* **2021**, *3*, e135. [[CrossRef](#)]
2. Rogdakis, K.; Karakostas, N.; Kymakis, E. Up-scalable emerging energy conversion technologies enabled by 2D materials: From miniature power harvesters towards grid-connected energy systems. *Energy Environ. Sci.* **2021**, *14*, 3352–3392. [[CrossRef](#)]
3. Detz, R.J.; Reek, J.N.H.; van der Zwaan, B.C.C. The future of solar fuels: When could they become competitive? *Energy Environ. Sci.* **2018**, *11*, 1653–1669. [[CrossRef](#)]
4. Gong, J.; Li, C.; Wasielewski, M.R. Advances in solar energy conversion. *Chem. Soc. Rev.* **2019**, *48*, 1862–1864. [[CrossRef](#)]
5. Rueda-Marquez, J.J.; Levchuk, I.; Fernández Ibañez, P.; Sillanpää, M. A critical review on application of photocatalysis for toxicity reduction of real wastewaters. *J. Clean. Prod.* **2020**, *258*, 120694. [[CrossRef](#)]
6. Xu, Y.-J. Promises and Challenges in Photocatalysis. *Front. Catal.* **2021**, *1*, 6. [[CrossRef](#)]
7. Bakbolat, B.; Daulbayev, C.; Sultanov, F.; Beissenov, R.; Umirzakov, A.; Mereke, A.; Bekbaev, A.; Chuprakov, I. Recent Developments of TiO₂-Based Photocatalysis in the Hydrogen Evolution and Photodegradation: A Review. *Nanomaterials* **2020**, *10*, 1790. [[CrossRef](#)] [[PubMed](#)]
8. Do, H.H.; Nguyen, D.L.T.; Nguyen, X.C.; Le, T.-H.; Nguyen, T.P.; Trinh, Q.T.; Ahn, S.H.; Vo, D.-V.N.; Kim, S.Y.; Van Le, Q. Recent progress in TiO₂-based photocatalysts for hydrogen evolution reaction: A review. *Arab. J. Chem.* **2020**, *13*, 3653–3671. [[CrossRef](#)]
9. Bokare, A.; Pai, M.; Athawale, A.A. Surface modified Nd doped TiO₂ nanoparticles as photocatalysts in UV and solar light irradiation. *Sol. Energy* **2013**, *91*, 111–119. [[CrossRef](#)]
10. Weon, S.; Choi, E.; Kim, H.; Kim, J.Y.; Park, H.-J.; Kim, S.-M.; Kim, W.; Choi, W. Active {001} Facet Exposed TiO₂ Nanotubes Photocatalyst Filter for Volatile Organic Compounds Removal: From Material Development to Commercial Indoor Air Cleaner Application. *Environ. Sci. Technol.* **2018**, *52*, 9330–9340. [[CrossRef](#)]

11. Chu, L.; Qin, Z.; Yang, J.; Li, X. Anatase TiO₂ Nanoparticles with Exposed {001} Facets for Efficient Dye-Sensitized Solar Cells. *Sci. Rep.* **2015**, *5*, 12143. [[CrossRef](#)]
12. Tachikawa, T.; Yamashita, S.; Majima, T. Evidence for crystal-face-dependent TiO₂ photocatalysis from single-molecule imaging and kinetic analysis. *J. Am. Chem. Soc.* **2011**, *133*, 7197–7204. [[CrossRef](#)]
13. Du, Y.-E.; Niu, X.; Li, W.; An, J.; Liu, Y.; Chen, Y.; Wang, P.; Yang, X.; Feng, Q. Microwave-Assisted Synthesis of High-Energy Faceted TiO₂ Nanocrystals Derived from Exfoliated Porous Metatitanic Acid Nanosheets with Improved Photocatalytic and Photovoltaic Performance. *Materials* **2019**, *12*, 3614. [[CrossRef](#)]
14. Liu, G.; Yang, H.G.; Pan, J.; Yang, Y.Q.; Lu, G.Q.M.; Cheng, H.-M. Titanium dioxide crystals with tailored facets. *Chem. Rev.* **2014**, *114*, 9559–9612. [[CrossRef](#)]
15. Andrés, J.; Gracia, L.; Gouveia, A.F.; Ferrer, M.M.; Longo, E. Effects of surface stability on the morphological transformation of metals and metal oxides as investigated by first-principles calculations. *Nanotechnology* **2015**, *26*, 405703. [[CrossRef](#)] [[PubMed](#)]
16. Martsinovich, N.; Troisi, A. How TiO₂ crystallographic surfaces influence charge injection rates from a chemisorbed dye sensitizer. *Phys. Chem. Chem. Phys.* **2012**, *14*, 13392–13401. [[CrossRef](#)]
17. Butburee, T.; Kotchasarn, P.; Hirunsit, P.; Sun, Z.; Tang, Q.; Khemthong, P.; Sangkhun, W.; Thongsuwan, W.; Kumnorkaew, P.; Wang, H.; et al. New understanding of crystal control and facet selectivity of titanium dioxide ruling photocatalytic performance. *J. Mater. Chem. A Mater. Energy Sustain.* **2019**, *7*, 8156–8166. [[CrossRef](#)]
18. Liu, X.; Du, G.; Li, M. True Photoreactivity Origin of Ti³⁺-Doped Anatase TiO₂ Crystals with Respectively Dominated Exposed {001}, {101}, and {100} Facets. *ACS Omega* **2019**, *4*, 14902–14912. [[CrossRef](#)]
19. Zheng, J.-Y.; Bao, S.-H.; Guo, Y.; Jin, P. Anatase TiO₂ films with dominant {001} facets fabricated by direct-current reactive magnetron sputtering at room temperature: Oxygen defects and enhanced visible-light photocatalytic behaviors. *ACS Appl. Mater. Interfaces* **2014**, *6*, 5940–5946. [[CrossRef](#)] [[PubMed](#)]
20. Yu, Y.; Wang, X.; Sun, H.; Ahmad, M. 3D anatase TiO₂ hollow microspheres assembled with high-energy {001} facets for lithium-ion batteries. *RSC Adv.* **2012**, *2*, 7901–7905. [[CrossRef](#)]
21. Niu, L.; Zhang, Q.; Liu, J.; Qian, J.; Zhou, X. TiO₂ nanoparticles embedded in hollow cube with highly exposed 001 facets: Facile synthesis and photovoltaic applications. *J. Alloys Compd.* **2016**, *656*, 863–870. [[CrossRef](#)]
22. Pei, D.-N.; Gong, L.; Zhang, A.-Y.; Zhang, X.; Chen, J.-J.; Mu, Y.; Yu, H.Q. Defective titanium dioxide single crystals exposed by high-energy {001} facets for efficient oxygen reduction. *Nat. Commun.* **2015**, *6*, 8696. [[CrossRef](#)]
23. Hu, C.; Zhang, X.; Li, W.; Yan, Y.; Xi, G.; Yang, H.; Yu, H.-Q. Large-scale, ultrathin and (001) facet exposed TiO₂ nanosheet superstructures and their applications in photocatalysis. *J. Mater. Chem. A Mater. Energy Sustain.* **2014**, *2*, 2040–2043. [[CrossRef](#)]
24. Umar, A.A.; Md Saad, S.K.; Ali Umar, M.I.; Rahman, M.Y.A.; Oyama, M. Advances in porous and high-energy (001)-faceted anatase TiO₂ nanostructures. *Opt. Mater.* **2018**, *75*, 390–430. [[CrossRef](#)]
25. Di Liberto, G.; Tosoni, S.; Pacchioni, G. Nitrogen doping in coexposed (001)-(101) anatase TiO₂ surfaces: A DFT study. *Phys. Chem. Chem. Phys.* **2019**, *21*, 21497–21505. [[CrossRef](#)]
26. Banerjee, B.; Amoli, V.; Maurya, A.; Sinha, A.K.; Bhaumik, A. Green synthesis of Pt-doped TiO₂ nanocrystals with exposed (001) facets and mesoscopic void space for photo-splitting of water under solar irradiation. *Nanoscale* **2015**, *7*, 10504–10512. [[CrossRef](#)] [[PubMed](#)]
27. Wei, Z.; Janczarek, M.; Endo, M.; Wang, K.; Balčytis, A.; Nitta, A.; Mendez-Medrano, M.-G.; Colbeau-Justin, C.; Juodkazis, S.; Othani, B.; et al. Noble metal-modified faceted anatase titania photocatalysts: Octahedron versus decahedron. *Appl. Catal. B* **2018**, *237*, 574–587. [[CrossRef](#)]
28. Lu, T.; Zhang, R.; Hu, C.; Chen, F.; Duo, S.; Hu, Q. TiO₂-graphene composites with exposed {001} facets produced by a one-pot solvothermal approach for high performance photocatalyst. *Phys. Chem. Chem. Phys.* **2013**, *15*, 12963–12970. [[CrossRef](#)] [[PubMed](#)]
29. Tang, B.; Chen, H.; Peng, H.; Wang, Z.; Huang, W. Graphene Modified TiO₂ Composite Photocatalysts: Mechanism, Progress and Perspective. *Nanomaterials* **2018**, *8*, 105. [[CrossRef](#)]
30. Ong, W.-J.; Tan, L.-L.; Chai, S.-P.; Yong, S.-T.; Mohamed, A.R. Facet-dependent photocatalytic properties of TiO₂-based composites for energy conversion and environmental remediation. *ChemSusChem* **2014**, *7*, 690–719. [[CrossRef](#)]
31. Chen, J.S.; Lou, X.W. SnO₂ and TiO₂ nanosheets for lithium-ion batteries. *Mater. Today* **2012**, *15*, 246–254. [[CrossRef](#)]
32. Kuang, Q.; Wang, X.; Jiang, Z.; Xie, Z.; Zheng, L. High-energy-surface engineered metal oxide micro- and nanocrystallites and their applications. *Acc. Chem. Res.* **2014**, *47*, 308–318. [[CrossRef](#)] [[PubMed](#)]
33. Lu, Y.; Zang, Y.; Zhang, H.; Zhang, Y.; Wang, G.; Zhao, H. Meaningful comparison of photocatalytic properties of {001} and {101} faceted anatase TiO₂ nanocrystals. *Sci. Bull. Fac. Agric. Kyushu Univ.* **2016**, *61*, 1003–1012.
34. Yang, J.; Wu, Q.; He, S.; Yan, J.; Shi, J.; Chen, J.; Wu, M.; Yang, X. Completely oriented anatase TiO₂ nanoarrays: Topotactic growth and orientation-related efficient photocatalysis. *Nanoscale* **2015**, *7*, 13888–13897. [[CrossRef](#)]
35. Xiong, Z.; Lei, Z.; Li, Y.; Dong, L.; Zhao, Y.; Zhang, J. A review on modification of facet-engineered TiO₂ for photocatalytic CO₂ reduction. *J. Photochem. Photobiol. C Photochem. Rev.* **2018**, *36*, 24–47. [[CrossRef](#)]
36. Maisano, M.; Dozzi, M.V.; Coduri, M.; Artiglia, L.; Granozzi, G.; Selli, E. Unraveling the Multiple Effects Originating the Increased Oxidative Photoactivity of {001}-Facet Enriched Anatase TiO₂. *ACS Appl. Mater. Interfaces* **2016**, *8*, 9745–9754. [[CrossRef](#)]
37. Dozzi, M.V.; Selli, E. Specific Facets-Dominated Anatase TiO₂: Fluorine-Mediated Synthesis and Photoactivity. *Catalysts* **2013**, *3*, 455–485. [[CrossRef](#)]

38. Vittadini, A.; Selloni, A.; Rotzinger, F.P.; Grätzel, M. Structure and Energetics of Water Adsorbed at TiO₂ Anatase (101) and (001) Surfaces. *Phys. Rev. Lett.* **1998**, *81*, 2954–2957. [[CrossRef](#)]
39. Selloni, A. Crystal growth: Anatase shows its reactive side. *Nat. Mater.* **2008**, *7*, 613–615. [[CrossRef](#)]
40. Liu, N.; Li, K.; Li, X.; Chang, Y.; Feng, Y.; Sun, X.; Cheng, Y.; Wu, Z.; Zhang, H. Crystallographic Facet-Induced Toxicological Responses by Faceted Titanium Dioxide Nanocrystals. *ACS Nano* **2016**, *10*, 6062–6073. [[CrossRef](#)]
41. Liu, N.; Chang, Y.; Feng, Y.; Cheng, Y.; Sun, X.; Jian, H.; Feng, Y.; Li, X.; Zhang, H. {101}-{001} Surface Heterojunction-Enhanced Antibacterial Activity of Titanium Dioxide Nanocrystals Under Sunlight Irradiation. *ACS Appl. Mater. Interfaces* **2017**, *9*, 5907–5915. [[CrossRef](#)]
42. Liu, S.; Yu, J.; Jaroniec, M. Anatase TiO₂ with dominant high-energy 001 facets: Synthesis, properties, and applications. *Chem. Mater.* **2011**, *23*, 4085–4093. [[CrossRef](#)]
43. Yang, H.G.; Sun, C.H.; Qiao, S.Z.; Zou, J.; Liu, G.; Smith, S.C.; Cheng, H.M.; Lu, G.Q. Anatase TiO₂ single crystals with a large percentage of reactive facets. *Nature* **2008**, *453*, 638–641. [[CrossRef](#)] [[PubMed](#)]
44. Liu, G.; Yang, H.G.; Wang, X.; Cheng, L.; Lu, H.; Wang, L.; Lu, G.Q.; Cheng, H.M. Enhanced Photoactivity of Oxygen-Deficient Anatase TiO₂ Sheets with Dominant {001} Facets. *J. Phys. Chem. C* **2009**, *113*, 21784–21788. [[CrossRef](#)]
45. Yang, P.; Douthwaite, M.; Pan, J.; Zheng, L.; Hong, S.; Morgan, D.J.; Gao, M.; Li, D.; Feng, J.; Hutchings, G.J. Coordinately unsaturated O_{2c}-Ti_{5c}-O_{2c} sites promote the reactivity of Pt/TiO₂ catalysts in the solvent-free oxidation of n-octanol. *Catal. Sci. Technol.* **2021**, *11*, 4898–4910. [[CrossRef](#)]
46. Ohno, T.; Sarukawa, K.; Matsumura, M. Crystal faces of rutile and anatase TiO₂ particles and their roles in photocatalytic reactions. *New J. Chem.* **2002**, *26*, 1167–1170. [[CrossRef](#)]
47. Li, J.; Niu, L.; He, X. Enhanced visible-light activity of Ti³⁺ self-doped TiO₂ with co-exposed 001 and 101 facets. *Micro Nano Lett.* **2018**, *13*, 514–517. [[CrossRef](#)]
48. Di Liberto, G.; Tosoni, S.; Pacchioni, G. Role of Heterojunction in Charge Carrier Separation in Coexposed Anatase (001)-(101) Surfaces. *J. Phys. Chem. Lett.* **2019**, *10*, 2372–2377. [[CrossRef](#)]
49. Murakami, N.; Kurihara, Y.; Tsubota, T.; Ohno, T. Shape-Controlled Anatase Titanium(IV) Oxide Particles Prepared by Hydrothermal Treatment of Peroxo Titanic Acid in the Presence of Polyvinyl Alcohol. *J. Phys. Chem. C* **2009**, *113*, 3062–3069. [[CrossRef](#)]
50. Ye, L.; Liu, J.; Tian, L.; Peng, T.; Zan, L. The replacement of {101} by {010} facets inhibits the photocatalytic activity of anatase TiO₂. *Appl. Catal. B* **2013**, *134–135*, 60–65. [[CrossRef](#)]
51. Zheng, Z.; Huang, B.; Lu, J.; Qin, X.; Zhang, X.; Dai, Y. Hierarchical TiO₂ microspheres: Synergetic effect of {001} and {101} facets for enhanced photocatalytic activity. *Chemistry* **2011**, *17*, 15032–15038. [[CrossRef](#)] [[PubMed](#)]
52. Wang, J.; Lin, W.; Zhou, S.; Li, Z.; Hu, H.; Tao, Y.; Zhou, S.; Zhao, X.; Kong, Y. Probing the formation and optical properties of Ti³⁺-TiO₂ with (001) exposed crystal facet by ethanol-assisted fluorination. *New J. Chem.* **2021**, *45*, 12453–12463. [[CrossRef](#)]
53. Liu, G.; Sun, C.; Yang, H.G.; Smith, S.C.; Wang, L.; Lu, G.Q.M.; Cheng, H.M. Nanosized anatase TiO₂ single crystals for enhanced photocatalytic activity. *Chem. Commun.* **2010**, *46*, 755–757. [[CrossRef](#)]
54. Angeline Dorothy, A.; Panigrahi, P. Tuning optical properties of TiO₂ by dimension reduction: From 3D bulk to 2D sheets along {001} and {101} plane. *Mater. Res. Express* **2020**, *6*, 1250f1. [[CrossRef](#)]
55. Zhu, J.; Wang, S.; Bian, Z.; Xie, S.; Cai, C.; Wang, J.; Yang, H.; Li, H. Solvothermally controllable synthesis of anatase TiO₂ nanocrystals with dominant {001} facets and enhanced photocatalytic activity. *CrystEngComm* **2010**, *12*, 2219–2224. [[CrossRef](#)]
56. Liu, S.; Yu, J.; Jaroniec, M. Tunable photocatalytic selectivity of hollow TiO₂ microspheres composed of anatase polyhedra with exposed {001} facets. *J. Am. Chem. Soc.* **2010**, *132*, 11914–11916. [[CrossRef](#)]
57. Amano, F.; Yasumoto, T.; Mahaney, O.O.P.; Uchida, S.; Shibayama, T.; Terada, Y.; Ohtani, B. Highly active Titania photocatalyst particles of controlled crystal phase, size, and polyhedral shapes. *Top. Catal.* **2010**, *53*, 455–461. [[CrossRef](#)]
58. Chen, J.S.; Tan, Y.L.; Li, C.M.; Cheah, Y.L.; Luan, D.; Madhavi, S.; Boey, F.Y.; Archer, L.A.; Lou, X.W. Constructing hierarchical spheres from large ultrathin anatase TiO₂ nanosheets with nearly 100% exposed (001) facets for fast reversible lithium storage. *J. Am. Chem. Soc.* **2010**, *132*, 6124–6130. [[CrossRef](#)] [[PubMed](#)]
59. Hengerer, R.; Kavan, L.; Krtil, P.; Grätzel, M. Orientation Dependence of Charge-Transfer Processes on TiO₂ (Anatase) Single Crystals. *J. Electrochem. Soc.* **2000**, *147*, 1467. [[CrossRef](#)]
60. Zhang, Y.; Tang, Y.; Li, W.; Chen, X. Nanostructured TiO₂-Based Anode Materials for High-Performance Rechargeable Lithium-Ion Batteries. *Chem. Nano. Mat.* **2016**, *2*, 764–775. [[CrossRef](#)]
61. Cheng, X.-L.; Hu, M.; Huang, R.; Jiang, J.-S. HF-free synthesis of anatase TiO₂ nanosheets with largely exposed and clean {001} facets and their enhanced rate performance as anodes of lithium-ion battery. *ACS Appl. Mater. Interfaces* **2014**, *6*, 19176–19183. [[CrossRef](#)]
62. Khlyustova, A.; Sirotkin, N.; Kusova, T.; Kraev, A.; Titov, V.; Agafonov, A. Doped TiO₂: The effect of doping elements on photocatalytic activity. *Mater. Adv.* **2020**, *1*, 1193–1201. [[CrossRef](#)]
63. Sulaiman, S.N.A.; Noh, M.Z.; Adnan, N.N.; Bidin, N.; Razak, S.N.A. Effects of photocatalytic activity of metal and non-metal doped TiO₂ for Hydrogen production enhancement—A Review. *J. Phys. Conf. Ser.* **2018**, *1027*, 012006. [[CrossRef](#)]
64. Rauf, M.A.; Meetani, M.A.; Hisaindee, S. An overview on the photocatalytic degradation of azo dyes in the presence of TiO₂ doped with selective transition metals. *Desalination* **2011**, *276*, 13–27. [[CrossRef](#)]

65. Mazierski, P.; Mikolajczyk, A.; Bajorowicz, B.; Malankowska, A.; Zaleska-Medynska, A.; Nadolna, J. The role of lanthanides in TiO₂-based photocatalysis: A review. *Appl. Catal. B* **2018**, *233*, 301–317. [[CrossRef](#)]
66. Zhu, Y.; Zhang, Z.; Lu, N.; Hua, R.; Dong, B. Prolonging charge-separation states by doping lanthanide-ions into {001}/{101} facets-coexposed TiO₂ nanosheets for enhancing photocatalytic H₂ evolution. *Chin. J. Catal.* **2019**, *40*, 413–423.
67. Zhang, J.; Xi, J.; Ji, Z. Mo + N Codoped TiO₂ sheets with dominant {001} facets for enhancing visible-light photocatalytic activity. *J. Mater. Chem.* **2012**, *22*, 17700–17708. [[CrossRef](#)]
68. Xiang, Q.; Yu, J.; Wang, W.; Jaroniec, M. Nitrogen self-doped nanosized TiO₂ sheets with exposed {001} facets for enhanced visible-light photocatalytic activity. *Chem. Commun.* **2011**, *47*, 6906–6908. [[CrossRef](#)]
69. Liu, G.; Sun, C.; Smith, S.C.; Wang, L.; Lu, G.Q.M.; Cheng, H.-M. Sulfur doped anatase TiO₂ single crystals with a high percentage of {001} facets. *J. Colloid Interface Sci.* **2010**, *349*, 477–483.
70. Shi, J.-W.; Liu, C.; He, C.; Li, J.; Xie, C.; Yang, S.; Chen, J.-W.; Li, S.; Niu, C. Carbon-doped titania nanoplates with exposed {001} facets: Facile synthesis, characterization and visible-light photocatalytic performance. *RSC Adv.* **2015**, *5*, 17667–17675.
71. Li, C.; Sun, Z.; Ma, R.; Xue, Y.; Zheng, S. Fluorine doped anatase TiO₂ with exposed reactive (001) facets supported on porous diatomite for enhanced visible-light photocatalytic activity. *Microporous Mesoporous Mater.* **2017**, *243*, 281–290. [[CrossRef](#)]
72. Dozzi, M.V.; Selli, E. Doping TiO₂ with p-block elements: Effects on photocatalytic activity. *J. Photochem. Photobiol. C Photochem. Rev.* **2013**, *14*, 13–28. [[CrossRef](#)]
73. Yalçın, Y.; Kılıç, M.; Çınar, Z. The Role of Non-Metal Doping in TiO₂ Photocatalysis. *J. Adv. Oxid. Technol.* **2010**, *13*, 281–296. [[CrossRef](#)]
74. González-Torres, J.C.; Poulain, E.; Domínguez-Soria, V.; García-Cruz, R.; Olvera-Neria, O. C-, N-, S-, and F-Doped Anatase TiO₂ (101) with Oxygen Vacancies: Photocatalysts Active in the Visible Region. *Int. J. Photoenergy* **2018**, *2018*, 7506151. [[CrossRef](#)]
75. Zhuang, H.; Zhang, Y.; Chu, Z.; Long, J.; An, X.; Zhang, H.; Lin, H.; Zhang, Z.; Wang, X. Synergy of metal and nonmetal dopants for visible-light photocatalysis: A case-study of Sn and N co-doped TiO₂. *Phys. Chem. Chem. Phys.* **2016**, *18*, 9636–9644. [[CrossRef](#)]
76. Suriyachai, N.; Chuangchote, S.; Laosiripojana, N.; Champreda, V.; Sagawa, T. Synergistic Effects of Co-Doping on Photocatalytic Activity of Titanium Dioxide on Glucose Conversion to Value-Added Chemicals. *ACS Omega* **2020**, *5*, 20373–20381. [[CrossRef](#)]
77. Xiang, Q.; Yu, J.; Jaroniec, M. Nitrogen and sulfur co-doped TiO₂ nanosheets with exposed {001} facets: Synthesis, characterization and visible-light photocatalytic activity. *Phys. Chem. Chem. Phys.* **2011**, *13*, 4853–4861. [[CrossRef](#)]
78. Zhang, Y.; Li, C.; Pan, C. N + Ni codoped anatase TiO₂ nanocrystals with exposed 001 facets through two-step hydrothermal route. *J. Am. Ceram. Soc.* **2012**, *95*, 2951–2956. [[CrossRef](#)]
79. Athawale, A.; Bokare, A.; Singh, H.; Nguyen, V.-H.; Sharma, A. Synthesis of Ag₂O Coated TiO₂ Nanoparticles by Sonochemically Activated Methods for Enhanced Photocatalytic Activities. *Top. Catal.* **2020**, *63*, 1056–1065. [[CrossRef](#)]
80. Sescu, A.M.; Favier, L.; Lutic, D.; Soto-Donoso, N.; Ciobanu, G.; Harja, M. TiO₂ Doped with Noble Metals as an Efficient Solution for the Photodegradation of Hazardous Organic Water Pollutants at Ambient Conditions. *Water* **2020**, *13*, 19.
81. Yu, J.; Qi, L.; Jaroniec, M. Hydrogen Production by Photocatalytic Water Splitting over Pt/TiO₂ Nanosheets with Exposed (001) Facets. *J. Phys. Chem. C* **2010**, *114*, 13118–13125. [[CrossRef](#)]
82. Yan, J.; Wu, G.; Dai, W.; Guan, N.; Li, L. Synthetic Design of Gold Nanoparticles on Anatase TiO₂ {001} for Enhanced Visible Light Harvesting. *ACS Sustain. Chem. Eng.* **2014**, *2*, 1940–1946. [[CrossRef](#)]
83. Lyu, Z.; Liu, B.; Wang, R.; Tian, L. Synergy of palladium species and hydrogenation for enhanced photocatalytic activity of {001} facets dominant TiO₂ nanosheets. *J. Mater. Res.* **2017**, *32*, 2781–2789. [[CrossRef](#)]
84. Kumar, S.; Kumar, A.; Bahuguna, A.; Sharma, V.; Krishnan, V. Two-dimensional carbon-based nanocomposites for photocatalytic energy generation and environmental remediation applications. *Beilstein J. Nanotechnol.* **2017**, *8*, 1571–1600. [[CrossRef](#)]
85. Lim, Y.; Lee, D.-K.; Kim, S.M.; Park, W.; Cho, S.Y.; Sim, U. Low Dimensional Carbon-Based Catalysts for Efficient Photocatalytic and Photo/Electrochemical Water Splitting Reactions. *Materials* **2019**, *13*, 114. [[CrossRef](#)] [[PubMed](#)]
86. Giovannetti, R.; Rommozzi, E.; Zannotti, M.; D’Amato, C.A. Recent Advances in Graphene Based TiO₂ Nanocomposites (GTiO₂Ns) for Photocatalytic Degradation of Synthetic Dyes. *Catalysts* **2017**, *7*, 305. [[CrossRef](#)]
87. Bokare, A.; Chinnusamy, S.; Erogbogbo, F. TiO₂-Graphene Quantum Dots Nanocomposites for Photocatalysis in Energy and Biomedical Applications. *Catalysts* **2021**, *11*, 319. [[CrossRef](#)]
88. Sun, W.; Wang, Y. Graphene-based nanocomposite anodes for lithium-ion batteries. *Nanoscale* **2014**, *6*, 11528–11552. [[CrossRef](#)]
89. Humayun, M.; Raziq, F.; Khan, A.; Luo, W. Modification strategies of TiO₂ for potential applications in photocatalysis: A critical review. *Green Chem. Lett. Rev.* **2018**, *11*, 86–102. [[CrossRef](#)]
90. Bokare, A.; Singh, H.; Pai, M.; Nair, R.; Sabharwal, S.; Athawale, A.A. Hydrothermal synthesis of Ag@TiO₂-Fe₃O₄ nanocomposites using sonochemically activated precursors: Magnetic, photocatalytic and antibacterial properties. *Mater. Res. Express* **2014**, *1*, 046111. [[CrossRef](#)]
91. Liu, L.; Gu, X.; Sun, C.; Li, H.; Deng, Y.; Gao, F.; Lin, D. In situ loading of ultra-small Cu₂O particles on TiO₂ nanosheets to enhance the visible-light photoactivity. *Nanoscale* **2012**, *4*, 6351–6359. [[CrossRef](#)] [[PubMed](#)]
92. Shen, J.; Zhu, Y.; Yang, X.; Li, C. Magnetic composite microspheres with exposed {001} faceted TiO₂ shells: A highly active and selective visible-light photocatalyst. *J. Mater. Chem.* **2012**, *22*, 13341–13347. [[CrossRef](#)]
93. Qi, L.; Yu, J.; Jaroniec, M. Preparation and enhanced visible-light photocatalytic H₂-production activity of CdS-sensitized Pt/TiO₂ nanosheets with exposed (001) facets. *Phys. Chem. Chem. Phys.* **2011**, *13*, 8915–8923. [[CrossRef](#)] [[PubMed](#)]

94. Moon, S.H.; Kim, M.J.; Im, S.H. Synthesis of lustering two-dimensional α - MoO_3 van der Waals crystals by TiO_2 assisted selective facet passivation. *J. Ind. Eng. Chem.* **2020**, *84*, 358–365. [[CrossRef](#)]
95. Chen, G.; Ji, S.; Li, H.; Kang, X.; Chang, S.; Wang, Y.; Yu, G.; Lu, J.; Claverie, J.; Sang, Y.; et al. High-Energy Faceted SnO_2 -Coated TiO_2 Nanobelt Heterostructure for Near-Ambient Temperature-Responsive Ethanol Sensor. *ACS Appl. Mater. Interfaces* **2015**, *7*, 24950–24956. [[CrossRef](#)]
96. Angel, R.D.; Durán-Álvarez, J.C.; Zanella, R. Photocatalysis. In *Titanium Dioxide*; Yang, D., Ed.; IntechOpen: Rijeka, Croatia, 2018.
97. Nguyen, C.K.; Cha, H.G.; Kang, Y.S. Axis-Oriented, Anatase TiO_2 Single Crystals with Dominant {001} and {100} Facets. *Cryst. Growth Des.* **2011**, *11*, 3947–3953. [[CrossRef](#)]
98. Yang, X.H.; Li, Z.; Sun, C.; Yang, H.G.; Li, C. Hydrothermal Stability of {001} Faceted Anatase TiO_2 . *Chem. Mater.* **2011**, *23*, 3486–3494. [[CrossRef](#)]
99. Barnard, A.S.; Curtiss, L.A. Prediction of TiO_2 nanoparticle phase and shape transitions controlled by surface chemistry. *Nano Lett.* **2005**, *5*, 1261–1266. [[CrossRef](#)]
100. Li, F.; Huang, Y.; Peng, H.; Cao, Y.; Niu, Y. Preparation and Photocatalytic Water Splitting Hydrogen Production of Titanium Dioxide Nanosheets. *Int. J. Photoenergy* **2020**, *2020*, 3617312. [[CrossRef](#)]
101. Liu, S.; Liu, B.; Nakata, K.; Ochiai, T.; Murakami, T.; Fujishima, A. Electrospinning Preparation and Photocatalytic Activity of Porous TiO_2 Nanofibers. *J. Nanomater.* **2012**, *2012*, 1–5. [[CrossRef](#)]
102. Yu, J.; Fan, J.; Lv, K. Anatase TiO_2 nanosheets with exposed (001) facets: Improved photoelectric conversion efficiency in dye-sensitized solar cells. *Nanoscale* **2010**, *2*, 2144–2149. [[CrossRef](#)]
103. Ding, S.; Chen, J.S.; Wang, Z.; Cheah, Y.L.; Madhavi, S.; Hu, X.; Lou, X.-W. TiO_2 hollow spheres with large amount of exposed (001) facets for fast reversible lithium storage. *J. Mater. Chem.* **2011**, *21*, 1677–1680. [[CrossRef](#)]
104. Ong, W.-J.; Tan, L.-L.; Chai, S.-P.; Yong, S.-T.; Mohamed, A.R. Highly reactive {001} facets of TiO_2 -based composites: Synthesis, formation mechanism and characterization. *Nanoscale* **2014**, *6*, 1946–2008. [[CrossRef](#)]
105. Yang, H.G.; Liu, G.; Qiao, S.Z.; Sun, C.H.; Jin, Y.G.; Smith, S.C.; Zou, J.; Cheng, H.-M.; Lu, G.-Q. Solvothermal synthesis and photoreactivity of anatase TiO_2 nanosheets with dominant {001} facets. *J. Am. Chem. Soc.* **2009**, *131*, 4078–4083. [[CrossRef](#)]
106. Sayed, M.; Pingfeng, F.; Khan, H.M.; Zhang, P. Effect of Isopropanol on Microstructure and Activity of TiO_2 Films with Dominant {001} Facets for Photocatalytic Degradation of Bezafibrate. *Int. J. Photoenergy* **2014**, *2014*, 490264. [[CrossRef](#)]
107. Han, X.; Kuang, Q.; Jin, M.; Xie, Z.; Zheng, L. Synthesis of titania nanosheets with a high percentage of exposed (001) facets and related photocatalytic properties. *J. Am. Chem. Soc.* **2009**, *131*, 3152–3153. [[CrossRef](#)]
108. Miao, J.; Liu, B. Anatase TiO_2 microspheres with reactive {001} facets for improved photocatalytic activity. *RSC Adv.* **2012**, *3*, 1222–1226. [[CrossRef](#)]
109. Ma, X.Y.; Chen, Z.G.; Hartono, S.B.; Jiang, H.B.; Zou, J.; Qiao, S.Z.; Yang, H.-G. Fabrication of uniform anatase TiO_2 particles exposed by {001} facets. *Chem. Commun.* **2010**, *46*, 6608–6610. [[CrossRef](#)]
110. Feng, J.; Yin, M.; Wang, Z.; Yan, S.; Wan, L.; Li, Z.; Yang, H.-G. Facile synthesis of anatase TiO_2 mesocrystal sheets with dominant {001} facets based on topochemical conversion. *CrystEngComm* **2010**, *12*, 3425–3429. [[CrossRef](#)]
111. Yu, J.; Xiang, Q.; Ran, J.; Mann, S. One-step hydrothermal fabrication and photocatalytic activity of surface-fluorinated TiO_2 hollow microspheres and tabular anatase single micro-crystals with high-energy facets. *CrystEngComm* **2010**, *12*, 872–879. [[CrossRef](#)]
112. Lai, Z.; Peng, F.; Wang, Y.; Wang, H.; Yu, H.; Liu, P.; Zhao, H. Low temperature solvothermal synthesis of anatase TiO_2 single crystals with wholly {100} and {001} faceted surfaces. *J. Mater. Chem.* **2012**, *22*, 23906–23912. [[CrossRef](#)]
113. Yu, H.; Tian, B.; Zhang, J. Layered TiO_2 composed of anatase nanosheets with exposed {001} facets: Facile synthesis and enhanced photocatalytic activity. *Chemistry* **2011**, *17*, 5499–5502. [[CrossRef](#)]
114. Han, X.; Wang, X.; Xie, S.; Kuang, Q.; Ouyang, J.; Xie, Z.; Zheng, L. Carbonate ions-assisted syntheses of anatase TiO_2 nanoparticles exposed with high energy (001) facets. *RSC Adv.* **2012**, *2*, 3251–3253. [[CrossRef](#)]
115. Dinh, C.-T.; Nguyen, T.-D.; Kleitz, F.; Do, T.-O. Shape-controlled synthesis of highly crystalline titania nanocrystals. *ACS Nano* **2009**, *3*, 3737–3743. [[CrossRef](#)]
116. Dai, Y.; Copley, C.M.; Zeng, J.; Sun, Y.; Xia, Y. Synthesis of anatase TiO_2 nanocrystals with exposed {001} facets. *Nano Lett.* **2009**, *9*, 2455–2459. [[CrossRef](#)]
117. Shan, G.-B.; Demopoulos, G.P. The synthesis of aqueous-dispersible anatase TiO_2 nanoplatelets. *Nanotechnology* **2010**, *21*, 025604. [[CrossRef](#)]
118. Zhao, Z.; Sun, Z.; Zhao, H.; Zheng, M.; Du, P.; Zhao, J.; Fan, H. Phase control of hierarchically structured mesoporous anatase TiO_2 microspheres covered with {001} facets. *J. Mater. Chem.* **2012**, *22*, 21965–21971. [[CrossRef](#)]
119. Roy, N.; Sohn, Y.; Pradhan, D. Synergy of low-energy {101} and high-energy {001} TiO_2 crystal facets for enhanced photocatalysis. *ACS Nano* **2013**, *7*, 2532–2540. [[CrossRef](#)]
120. Li, J.; Yu, Y.; Chen, Q.; Li, J.; Xu, D. Controllable Synthesis of TiO_2 Single Crystals with Tunable Shapes Using Ammonium-Exchanged Titanate Nanowires as Precursors. *Cryst. Growth Des.* **2010**, *10*, 2111–2115. [[CrossRef](#)]
121. Li, T.; Tian, B.; Zhang, J.; Dong, R.; Wang, T.; Yang, F. Facile Tailoring of Anatase TiO_2 Morphology by Use of H_2O_2 : From Microflowers with Dominant {101} Facets to Microspheres with Exposed {001} Facets. *Ind. Eng. Chem. Res.* **2013**, *52*, 6704–6712. [[CrossRef](#)]

122. Amano, F.; Prieto-Mahaney, O.-O.; Terada, Y.; Yasumoto, T.; Shibayama, T.; Ohtani, B. Decahedral Single-Crystalline Particles of Anatase Titanium(IV) Oxide with High Photocatalytic Activity. *Chem Mater.* **2009**, *21*, 2601–2603. [[CrossRef](#)]
123. Jung, M.-H.; Chu, M.-J.; Kang, M.G. TiO₂ nanotube fabrication with highly exposed (001) facets for enhanced conversion efficiency of solar cells. *Chem. Commun.* **2012**, *48*, 5016–5018. [[CrossRef](#)]
124. Lee, W.-J.; Sung, Y.-M. Synthesis of Anatase Nanosheets with Exposed (001) Facets via Chemical Vapor Deposition. *Cryst. Growth Des.* **2012**, *12*, 5792–5795. [[CrossRef](#)]
125. Liu, G.; Yang, H.G.; Wang, X.; Cheng, L.; Pan, J.; Lu, G.Q.M.; Cheng, H.-M. Visible light responsive nitrogen doped anatase TiO₂ sheets with dominant {001} facets derived from TiN. *J. Am. Chem. Soc.* **2009**, *131*, 12868–12869. [[CrossRef](#)] [[PubMed](#)]
126. Yu, J.; Dai, G.; Xiang, Q.; Jaroniec, M. Fabrication and enhanced visible-light photocatalytic activity of carbon self-doped TiO₂ sheets with exposed {001} facets. *J. Mater. Chem.* **2011**, *21*, 1049–1057. [[CrossRef](#)]
127. Wu, X.-F.; Song, H.-Y.; Yoon, J.-M.; Yu, Y.-T.; Chen, Y.-F. Synthesis of core-shell Au@TiO₂ nanoparticles with truncated wedge-shaped morphology and their photocatalytic properties. *Langmuir* **2009**, *25*, 6438–6447. [[CrossRef](#)]
128. Liu, B.; Huang, Y.; Wen, Y.; Du, L.; Zeng, W.; Shi, Y.; Zhang, F.; Zhu, G.; Xu, X.; Wang, Y. Highly dispersive {001} facets-exposed nanocrystalline TiO₂ on high quality graphene as a high performance photocatalyst. *J. Mater. Chem.* **2012**, *22*, 7484–7491. [[CrossRef](#)]
129. Chinnusamy, S.; Kaur, R.; Bokare, A.; Erogbogbo, F. Incorporation of graphene quantum dots to enhance photocatalytic properties of anatase TiO₂. *MRS Commun.* **2018**, *8*, 137–144. [[CrossRef](#)]
130. Xiang, Q.; Yu, J.; Jaroniec, M. Enhanced photocatalytic H₂-production activity of graphene-modified titania nanosheets. *Nanoscale* **2011**, *3*, 3670–3678. [[CrossRef](#)]
131. Sun, L.; Zhao, Z.; Zhou, Y.; Liu, L. Anatase TiO₂ nanocrystals with exposed {001} facets on graphene sheets via molecular grafting for enhanced photocatalytic activity. *Nanoscale* **2012**, *4*, 613–620. [[CrossRef](#)]
132. Wang, W.-S.; Wang, D.-H.; Qu, W.-G.; Lu, L.-Q.; Xu, A.-W. Large Ultrathin Anatase TiO₂ Nanosheets with Exposed {001} Facets on Graphene for Enhanced Visible Light Photocatalytic Activity. *J. Phys. Chem. C* **2012**, *116*, 19893–19901. [[CrossRef](#)]
133. Jiang, B.; Tian, C.; Pan, Q.; Jiang, Z.; Wang, J.-Q.; Yan, W.; Honggang, F. Enhanced Photocatalytic Activity and Electron Transfer Mechanisms of Graphene/TiO₂ with Exposed {001} Facets. *J. Phys. Chem. C* **2011**, *115*, 23718–23725. [[CrossRef](#)]
134. Qiu, B.; Xing, M.; Zhang, J. Mesoporous TiO₂ nanocrystals grown in situ on graphene aerogels for high photocatalysis and lithium-ion batteries. *J. Am. Chem. Soc.* **2014**, *136*, 5852–5855. [[CrossRef](#)]
135. Chen, L.; Yang, S.; Zhang, Q.; Zhu, J.; Zhao, P. Rational design of {001}-faceted TiO₂ nanosheet arrays/graphene foam with superior charge transfer interfaces for efficient photocatalytic degradation of toxic pollutants. *Sep. Purif. Technol.* **2021**, *265*, 118444. [[CrossRef](#)]
136. Liu, H.; Li, P.; Bai, H.; Du, C.; Wei, D.; Su, Y.; Wang, Y.; Yang, L. Incorporation of reduced graphene oxide into faceted flower-like {001} TiO₂ for enhanced photocatalytic activity. *R. Soc. Open Sci.* **2018**, *5*, 180613. [[CrossRef](#)]
137. Thien, G.S.H.; Omar, F.S.; Blya, N.I.S.A.; Chiu, W.S.; Lim, H.N.; Yousefi, R.; Sheini, F.-J.; Huang, N.-M. Improved Synthesis of Reduced Graphene Oxide-Titanium Dioxide Composite with Highly Exposed 001 Facets and Its Photoelectrochemical Response. *Int. J. Photoenergy* **2014**, *2014*, 650583. [[CrossRef](#)]
138. Sui, Y.; Wu, L.; Zhong, S.; Liu, Q. Carbon quantum dots/TiO₂ nanosheets with dominant (001) facets for enhanced photocatalytic hydrogen evolution. *Appl. Surf. Sci.* **2019**, *480*, 810–816. [[CrossRef](#)]
139. Guo, W.; Zhang, F.; Lin, C.; Wang, Z.L. Direct growth of TiO₂ nanosheet arrays on carbon fibers for highly efficient photocatalytic degradation of methyl orange. *Adv. Mater.* **2012**, *24*, 4761–4764. [[CrossRef](#)]
140. Liu, Z.; Zheng, H.; Yang, H.; Hao, L.; Wen, L.; Xu, T.; Wu, S. mpg-C₃N₄/anatase TiO₂ with reactive {001} facets composites to enhance the photocatalytic activity of organic dye degradation. *RSC Adv.* **2016**, *6*, 54215–54225. [[CrossRef](#)]
141. Wang, W.; Ni, Y.R.; Lu, C.H.; Xu, Z.Z. Coupling {001} Facets Dominated Anatase TiO₂ Nanosheets with CNTs for Efficient Photocatalyst. *Adv. Mater. Res.* **2014**, *853*, 111–115. [[CrossRef](#)]
142. Chen, J.S.; Chen, C.; Liu, J.; Xu, R.; Qiao, S.Z.; Lou, X.W. Ellipsoidal hollow nanostructures assembled from anatase TiO₂ nanosheets as a magnetically separable photocatalyst. *Chem Commun.* **2011**, *47*, 2631–2633. [[CrossRef](#)]
143. Yue, X.; Zhang, J.; Yan, F.; Wang, X.; Huang, F. A situ hydrothermal synthesis of SrTiO₃/TiO₂ heterostructure nanosheets with exposed (001) facets for enhancing photocatalytic degradation activity. *Appl. Surf. Sci.* **2014**, *319*, 68–74. [[CrossRef](#)]
144. Li, S.; Zhu, G.; Jia, Y.; Pan, L.; Nie, J.; Rao, F.; Gao, J.; Zhang, F.; Kwon, N.; Liu, C. TiO₂ with exposed (001) facets/Bi₄O₅Br₂ nanosheets heterojunction with enhanced photocatalytic for NO removal. *Nanotechnology* **2020**, *31*, 254002. [[CrossRef](#)]
145. Crake, A.; Christoforidis, K.C.; Godin, R.; Moss, B.; Kafizas, A.; Zafeiratos, S.; Durrant, J.-R.; Petit, C. Titanium dioxide/carbon nitride nanosheet nanocomposites for gas phase CO₂ photoreduction under UV-visible irradiation. *Appl. Catal. B* **2019**, *242*, 369–378. [[CrossRef](#)]
146. Wang, S.; Xu, M.; Peng, T.; Zhang, C.; Li, T.; Hussain, I.; Wang, J.; Tan, B. Porous hypercrosslinked polymer-TiO₂-graphene composite photocatalysts for visible-light-driven CO₂ conversion. *Nat. Commun.* **2019**, *10*, 676. [[CrossRef](#)] [[PubMed](#)]
147. Ong, W.-J.; Tan, L.-L.; Chai, S.-P.; Yong, S.-T.; Mohamed, A.R. Self-assembly of nitrogen-doped TiO₂ with exposed {001} facets on a graphene scaffold as photo-active hybrid nanostructures for reduction of carbon dioxide to methane. *Nano Res.* **2014**, *7*, 1528–1547. [[CrossRef](#)]
148. Liu, X.; Cong, R.; Cao, L.; Liu, S.; Cui, H. The structure, morphology and photocatalytic activity of graphene-TiO₂ multilayer films and charge transfer at the interface. *New J. Chem.* **2014**, *38*, 2362–2367. [[CrossRef](#)]

149. Zhu, J.; Xiao, P.; Li, H.; Carabineiro, S.A.C. Graphitic carbon nitride: Synthesis, properties, and applications in catalysis. *ACS Appl. Mater. Interfaces* **2014**, *6*, 16449–16465. [[CrossRef](#)]
150. Manthiram, A. An Outlook on Lithium Ion Battery Technology. *ACS Cent. Sci.* **2017**, *3*, 1063–1069. [[CrossRef](#)]
151. Kim, T.; Song, W.; Son, D.-Y.; Ono, L.K.; Qi, Y. Lithium-ion batteries: Outlook on present, future, and hybridized technologies. *J. Mater. Chem. A Mater. Energy Sustain.* **2019**, *7*, 2942–2964. [[CrossRef](#)]
152. Diouf, B.; Pode, R. Potential of lithium-ion batteries in renewable energy. *Renew. Energy* **2015**, *76*, 375–380. [[CrossRef](#)]
153. Dufo-López, R.; Cortés-Arcos, T.; Artal-Sevil, J.S.; Bernal-Agustín, J.L. Comparison of Lead-Acid and Li-Ion Batteries Lifetime Prediction Models in Stand-Alone Photovoltaic Systems. *NATO Adv. Sci. Inst. Ser. E Appl. Sci.* **2021**, *11*, 1099.
154. Deng, D. Li-ion batteries: Basics, progress, and challenges. *Energy Sci. Eng.* **2015**, *3*, 385–418. [[CrossRef](#)]
155. Pradeep, N.; Sivasenthil, E.; Janarthanan, B.; Sharmila, S. A Review of Anode Material for Lithium Ion Batteries. *J. Phys. Conf. Ser.* **2019**, *1362*, 012026. [[CrossRef](#)]
156. Manthiram, A. A reflection on lithium-ion battery cathode chemistry. *Nat. Commun.* **2020**, *11*, 1550. [[CrossRef](#)] [[PubMed](#)]
157. Yao, P.; Yu, H.; Ding, Z.; Liu, Y.; Lu, J.; Lavorgna, M.; Wu, J.; Liu, X. Review on Polymer-Based Composite Electrolytes for Lithium Batteries. *Front. Chem.* **2019**, *7*, 522. [[CrossRef](#)]
158. Wang, L.; Li, J.; Lu, G.; Li, W.; Tao, Q.; Shi, C.; Jin, H.; Chen, G.; Wang, S. Fundamentals of Electrolytes for Solid-State Batteries: Challenges and Perspectives. *Front. Mater.* **2020**, *7*, 111. [[CrossRef](#)]
159. Liu, Y.; Yang, Y. Recent Progress of TiO₂-Based Anodes for Li Ion Batteries. *J. Nanomater.* **2016**, *2016*, 8123652. [[CrossRef](#)]
160. Yan, X.; Wang, Z.; He, M.; Hou, Z.; Chen, X. TiO₂ Nanomaterials as Anode Materials for Lithium-Ion Rechargeable Batteries. *Energy Technol.* **2015**, *3*, 801–814. [[CrossRef](#)]
161. Song, T.; Paik, U. TiO₂ as an active or supplemental material for lithium batteries. *J. Mater. Chem. A Mater. Energy Sustain.* **2015**, *4*, 14–31. [[CrossRef](#)]
162. Yu, W.-B.; Hu, Z.-Y.; Jin, J.; Yi, M.; Yan, M.; Li, Y.; Wang, H.-E.; Gao, H.-X.; Mai, L.-Q.; Hasan, T.; et al. Unprecedented and highly stable lithium storage capacity of (001) faceted nanosheet-constructed hierarchically porous TiO₂/rGO hybrid architecture for high-performance Li-ion batteries. *Natl. Sci. Rev.* **2020**, *7*, 1046–1058. [[CrossRef](#)]
163. Wang, Z.; Zhang, Y.; Xia, T.; Murowchick, J.; Liu, G.; Chen, X. Lithium-ion battery performance of (001)-faceted TiO₂ Nanosheets vs. Spherical TiO₂ Nanoparticles. *Energy Technol.* **2014**, *2*, 376–382. [[CrossRef](#)]
164. Sun, C.H.; Yang, X.H.; Chen, J.S.; Li, Z.; Lou, X.W.; Li, C.; Smith, S.-C.; Lu, G.-Q.; Yang, H.-G. Higher charge/discharge rates of lithium-ions across engineered TiO₂ surfaces leads to enhanced battery performance. *Chem. Commun.* **2010**, *46*, 6129–6131. [[CrossRef](#)]
165. Liu, J.; Chen, J.S.; Wei, X.; Lou, X.W.; Liu, X.-W. Sandwich-like, stacked ultrathin titanate nanosheets for ultrafast lithium storage. *Adv. Mater.* **2011**, *23*, 998–1002. [[CrossRef](#)]
166. Tao, H.-C.; Fan, L.-Z.; Yan, X.; Qu, X. In situ synthesis of TiO₂-graphene nanosheets composites as anode materials for high-power lithium ion batteries. *Electrochim. Acta* **2012**, *69*, 328–333. [[CrossRef](#)]
167. Zheng, P.; Liu, T.; Su, Y.; Zhang, L.; Guo, S. TiO₂ nanotubes wrapped with reduced graphene oxide as a high-performance anode material for lithium-ion batteries. *Sci. Rep.* **2016**, *6*, 36580. [[CrossRef](#)]
168. Chen, J.S.; Luan, D.; Li, C.M.; Boey, F.Y.C.; Qiao, S.; Lou, X.W. TiO₂ and SnO₂@TiO₂ hollow spheres assembled from anatase TiO₂ nanosheets with enhanced lithium storage properties. *Chem. Commun.* **2010**, *46*, 8252–8254. [[CrossRef](#)]
169. Chen, J.S.; Wen, X.; Lou, D. Unusual rutile TiO₂ nanosheets with exposed (001) facets. *Chem. Sci.* **2011**, *2*, 2219–2223. [[CrossRef](#)]
170. Ding, S.; Chen, J.S.; David Lou, X.W. One-dimensional hierarchical structures composed of novel metal oxide nanosheets on a carbon nanotube backbone and their lithium-storage properties. *Adv. Funct. Mater.* **2011**, *21*, 4120–4125. [[CrossRef](#)]
171. Liu, G.; Yin, L.-C.; Pan, J.; Li, F.; Wen, L.; Zhen, C.; Cheng, H.-M. Greatly Enhanced Electronic Conduction and Lithium Storage of Faceted TiO₂ Crystals Supported on Metallic Substrates by Tuning Crystallographic Orientation of TiO₂. *Adv. Mater.* **2015**, *27*, 3507–3512. [[CrossRef](#)]
172. Chen, J.S.; Liu, H.; Qiao, S.Z.; Lou, X.W. Carbon-supported ultra-thin anatase TiO₂ nanosheets for fast reversible lithium storage. *J. Mater. Chem.* **2011**, *21*, 5687–5692. [[CrossRef](#)]